2017

POTENTIAL FIELD MODELING ACROSS THE NEODYMIUM LINE DEFINING THE PALEOPROTEROZOIC-MESOPROTEROZOIC BOUNDARY OF THE SOUTHEASTERN MARGIN OF LAURENTIA

Rachel Lauren Durham
University of Kentucky, rldu232@uky.edu
Digital Object Identifier: https://doi.org/10.13023/ETD.2017.412

STUDENT AGREEMENT:

I represent that my thesis or dissertation and abstract are my original work. Proper attribution has been given to all outside sources. I understand that I am solely responsible for obtaining any needed copyright permissions. I have obtained needed written permission statement(s) from the owner(s) of each third-party copyrighted matter to be included in my work, allowing electronic distribution (if such use is not permitted by the fair use doctrine) which will be submitted to UKnowledge as Additional File.

I hereby grant to The University of Kentucky and its agents the irrevocable, non-exclusive, and royalty-free license to archive and make accessible my work in whole or in part in all forms of media, now or hereafter known. I agree that the document mentioned above may be made available immediately for worldwide access unless an embargo applies.

I retain all other ownership rights to the copyright of my work. I also retain the right to use in future works (such as articles or books) all or part of my work. I understand that I am free to register the copyright to my work.

REVIEW, APPROVAL AND ACCEPTANCE

The document mentioned above has been reviewed and accepted by the student's advisor, on behalf of the advisory committee, and by the Director of Graduate Studies (DGS), on behalf of the program; we verify that this is the final, approved version of the student's thesis including all changes required by the advisory committee. The undersigned agree to abide by the statements above.

Rachel Lauren Durham, Student

Dr. Dhananjay Ravat, Major Professor

Dr. Edward Woolery, Director of Graduate Studies

POTENTIAL FIELD MODELING ACROSS THE NEODYMIUM LINE DEFINING THE PALEOPROTEROZOIC-MESOPROTEROZOIC BOUNDARY OF THE SOUTHEASTERN MARGIN OF LAURENTIA

THESIS

A Thesis submitted in partial fulfillment of the
requirements for the degree of Master of Science in Geology
in the College of Arts and Sciences
at the University of Kentucky

By

Rachel Lauren Durham

Lexington, Kentucky

Director: Dr. Dhananjay Ravat, Professor of Geophysics

Lexington, Kentucky

2017

ABSTRACT OF THESIS

POTENTIAL FIELD MODELING ACROSS THE NEODYMIUM LINE DEFINING THE PALEOPROTEROZOIC-MESOPROTEROZOIC BOUNDARY OF THE SOUTHEASTERN MARGIN OF LAURENTIA

A zone of high magnetization along the SE margin of Paleoproterozoic Laurentia in the United States is indicated by magnetic anomaly data. The SE edge corresponds to the geochemical Neodymium mantle derivation model age (T_{DM}) boundary and the entire anomaly overlies the Paleoproterozoic Mazatzal Province. Two-dimensional gravity and magnetic models across the Nd boundary are created with Moho constrained from receiver functions with gravity, sedimentary thickness and the base of the crustal magnetization. Upper crustal magnetization does not show strong variation across this boundary and much of the strong magnetization appears to lie in the middle crust. Using magnetic modeling of several potential geologic scenarios, we estimate magnetization, depth extent, and width of this zone of high magnetization. The anomaly has variable width (~ 300 km) with amplitude of approximately 200 nT. Pre-1.55Ga Paleoproterozoic mid crustal blocks have significantly higher average effective susceptibility (0.06 SI) than those of the post-1.55Ga Mesoproterozoic (0.01 SI). In two of the three profiles, the Paleoproterozoic zone of high magnetization has the highest average susceptibility indicating the Mazatzal province is innately highly magnetic. The zone may have formed either by magmatism associated with westward subduction or from highly magnetic terranes wedging between accreting island arcs.

KEYWORDS: Geophysics, Geomagnetic Anomalies of the Laurentian Craton, Geochemistry of the Midcontinent United States, Two-Dimensional Potential Field Modeling, Forward Modeling

Rachel Lauren Durham

28 September, 2017

POTENTIAL FIELD MODELING ACROSS THE NEODYMIUM LINE DEFINING THE PALEOPROTEROZOIC-MESOPROTEROZOIC BOUNDARY OF THE SOUTHEASTERN MARGIN OF LAURENTIA

By

Rachel Lauren Durham

Dhananjay Ravat
Director of Thesis

Edward Woolery
Director of Graduate Studies

28 September, 2017

Acknowledgments

Foremost I would like to thank my advisor Dr. Dhananjay Ravat for his guidance, support, and confidence in me throughout the entirety of this degree. His knowledge of geophysics and geophysical modeling contributed immensely in the completion of this thesis. I would also like to thank Dr. David Moecher who was instrumental in providing direction for knitting together the geophysical and geochemical aspects of this research. Additionally, I would like to thank my committee members Dr. Edward Woolery, Dr. Keely O'Farrell, and Dr. David Clark for their comments and suggestions for improvement in both this thesis and research in general. Dr. Henglei Zhang directly provided a necessary dataset for completion of this research, without it I would have lacked a critical constraint.

In addition to all of the academic help and support I received, I would also like to thank the department of Earth and Environmental Sciences for their continued support as a teaching assistant and for providing the Brown-McFarlan Fund. NSF grant 1246921 and NASA grants NNX16AJ99G and NNX16AN51G have been instrumental in facilitating my research endeavors throughout grad school.

Finally, I would like to thank my parents, Laurie and Danny, my boyfriend Glen, and all of my friends who have helped me and stood by me through all of the research and finally the thesis.

Table of Contents

List of Tables

List of Figures

Chapter 1 Introduction

A region of complexity that has undergone repeated deformation and tectonism for the last several billion years, the Laurentian Craton formed as an amalgamation of Archean blocks at its core and expanded by continental accretion through successive orogenies (Whitmeyer and Karlstrom, 2007). A region of particular interest within the craton that has seen more scrutiny in recent years, due to revisiting past unpublished data, is the midcontinent United States (Bickford et al., 2015).

Obscured by Paleozoic sediment deposition, where outcrops and boreholes are scarce, the origins of the cratonic core of the midcontinent of the United States have proven difficult to decipher. Geochemistry of relatively small sample size for this region has provided insights into the provenance of the midcontinent through Samarium-Neodymium model age dating (T_{DM}) and zircon radiometric dating (Bickford et al., 2015; Slagstad et al., 2009; Van Schmus et al., 1996).

A core built of Archean-aged Slave, Rae, and Hearne blocks in the north to the Superior, Wyoming, and Medicine Hat cratons in the south and east, was eventually sutured together into Laurentia by the 1.8-1.9 Ga Trans-Hudson Orogeny (Figure 1.1). After the accretion of Paleoproterozoic arc material spanning approximately 1.8-1.6 Ga, Laurentia underwent magmatism in the form of large provinces of granites and rhyolites on its southeastern and southern margins. Some of the most perplexing geologic provinces in the region comprise the Eastern and Southern Granite-Rhyolite (EGR, SGR, respectively) provinces. Multiple theories have been posited on their origin without a final consensus. Theories for formation of Granite-Rhyolite provinces and anorogenic (A-type) plutons seen laced throughout the region range from mantle interaction resulting in mafic underplating and consequent melting of lower crust to rift-related magmatism (Bickford et al., 2015; Slagstad et al., 2009; Van Schmus et al., 1996). Based on Nd-Sm model ages, approximately 1.55 billion years ago, Mesoproterozoic island arcs collided with the Paleoproterozoic margin of North America forming a suture zone extending from Texas northeastward through Michigan to the Canadian province of Labrador (Van Schmus et al., 1996). The extensive Eastern (1.45 Ga) and Southern (1.35 Ga) Granite-Rhyolite provinces, which represent partial melting of the lower crust, straddle the Proterozoic boundary and thus the collision of the landmasses may be diachronous and

must have occurred prior to their radiometric ages, i.e., prior to1.45 Ga in the north and 1.35 Ga in the south.

A magnetization high is observed along the Paleoproterozoic side of this inferred suture (Figure 1.2). This long-wavelength magnetic high was previously thought to originate in the lower crust as lower crust is generally more mafic (Ravat, 2007); however, recent spectral magnetic determinations of the base of crustal magnetization suggest that, for the most part, over large portions of the Paleoproterozoic province where the magnetization high lies, the lower crust is either nonmagnetic or very weakly magnetic (Ravat et al., 2015). Thus, the source regions of the long-wavelength magnetization high must be in the upper mantle or upper and middle crystalline crust.

The Nd line was originally defined based on sparse T_{DM} geochemical data (Van Schmus et al., 1996) and then later refined to include previously unpublished data (Bickford et al., 2015) (Figure 1.3). Surprisingly, the Nd line does not illustrate the aforementioned diachronous collision through continuous younging of ages from north to south (Bickford et al., 2015) but it does show a distinct difference in ages from the northwest to the southeast. The magnetization high occurs primarily over the 1.7-1.6 Ga Paleoproterozoic Mazatzal province on the northwestern side of the Nd line. Prior to recognition of the magnetization high, no geophysical contrast was known to be associated with the Nd line (Ravat, 2007; Bickford et al., 2015; Figure 1.2).

Magnetic anomaly data obtained from the CHAMP satellite magnetic field model MF7 is inverted to obtain effective susceptibility variation. Several features of the midcontinent United States become apparent from this susceptibility map (Figure 1.2). In Figure 1.2, the Midcontinent Rift of the Great Lakes region and several Archean blocks such as the Wyoming craton and Medicine Hat block show prominent high magnetization. Understanding the origin of the Mazatzal high magnetization zone and its relationship to the Nd line, Yavapai, and Mesoproterozoic provinces is the objective of this work.

Investigation of origin of such a high magnitude and expanse anomaly in a region as complex and large as the southeastern margin of Laurentia is encumbered by numerous obstacles because of non-uniqueness in potential fields. However, due to EarthScope Trasportable Array deployment and the analysis of the data using seismic

receiver-functions, the crustal thickness and Vp/Vs ratio (a proxy for rock types) have been more accurately constrained (results provided by A.R. Lowry, 2016, pers. comm.). These data combined with the sedimentary thickness derived from boreholes and information from key seismic refraction experiments provide constraints for modeling and interpreting the potential field anomalies in this region that has few rock exposures.

Interestingly enough, the zone of high magnetization is not accompanied by a zone of high gravity anomalies; however, a further constraint is provided by the depth to the base of crustal magnetization determined through the use of the de-fractal method of spectral magnetic depth determination (D. Ravat, 2016, pers. comm.).

In order to understand the potential sources of this zone of high magnetization in the region, magnetic and gravity models of several crustal sections across the Nd line were formed based on different scenarios that could have led to its formation. Several possible scenarios (discussed below) were developed for the zone of high magnetization based on the inferred geologic evolution of the region. The list was subsequently narrowed down to the most probable given the reasonability of derived magnetization and the processes that could have caused it. Additionally, a revised subduction scenario was created in order to illustrate the tectonic setting necessary for formation of a zone of high magnetization (Figure 1.4). Subducting plates that experience a polarity swap (a change in the subduction direction) has long been the preferred model of arc accretion onto the Laurentia margin; however, formation of the zone of high magnetization requires westward-dipping subduction in order to produce the magnetic high on the cratonic side of collision.

In present day oceanic-continental subduction settings, such as the Cascades Arc in the American Pacific Northwest, a zone of high magnetization accompanied by a lack of high gravity can be found inboard of the trench. This zone is interpreted to be the result of serpentinization of the forearc mantle through the metasomatization of mantle peridotite into serpentinite (Blakely et al., 2005). This process would lead to the formation of magnetite but, due to the low-density nature of serpentinite, leads to a complex gravity anomaly signature as a result of the effect of neighboring sources (Blakely et al., 2005; Bostock et al., 2002; Hyndman and Peacock, 2003). This setting is similar to the wide and high magnetization region in the midcontinent and thus consistent

with a mantle wedge in a subduction scenario. The biggest challenge for this hypothesis is the survival of the high magnetization in the mantle during its 1.5 Ga of geologic evolution.

Another geophysical feature seen in subduction settings and one of interest to this study is basaltic underplating of the lower crust. This scenario could provide an additional source of magnetization from Moho depths to bolster that already present in the middle and upper crust. If extant, the zone of basaltic underplating should appear in the seismic receiver function results as deepened Moho (because its seismic velocity and density would be similar to lower crust) and have a noticeable effect on the gravity anomalies of the region.

Aside from the previously discussed mantle sources of magnetization, crust-only magnetization will also be considered. Because the zone of high magnetization overlies the Mazatzal province, a province supposedly composed of primarily juvenile, mafic, and greenstone material (Amato et al., 2008; Whitmeyer and Karlstrom, 2007), another scenario will be examined that highlights the basement of this province having rocks made up of strongly magnetized minerals. This model will use the defractal method's base of magnetization without any mantle magnetic sources.

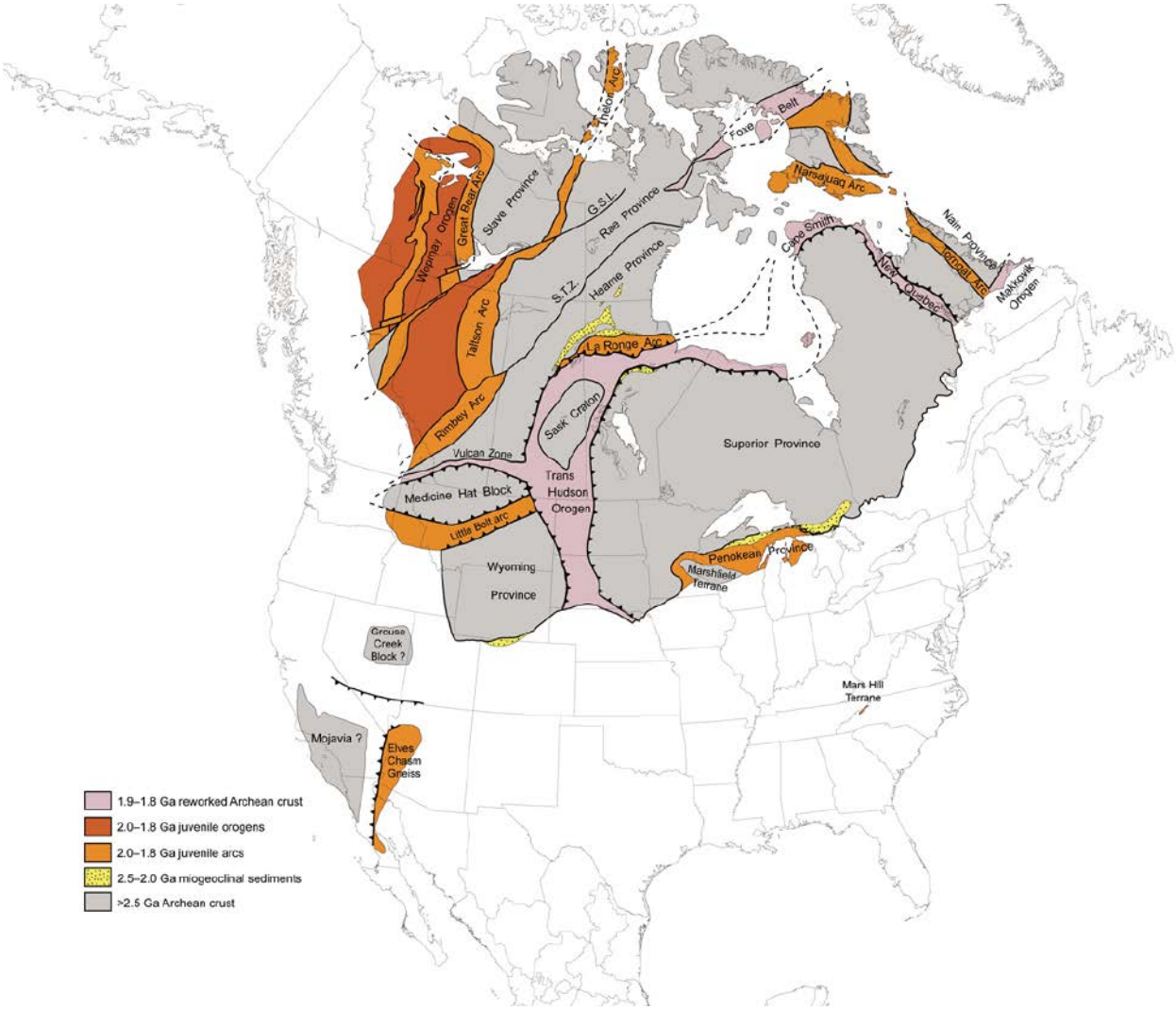

Figure 1.1 Amalgamation of Archean blocks to form the core of Laurentia. G.S.L. – Great Slave Lake shear zone, S.T.Z. – Snowbird tectonic zone (Whitmeyer and Karlstrom, 2007).

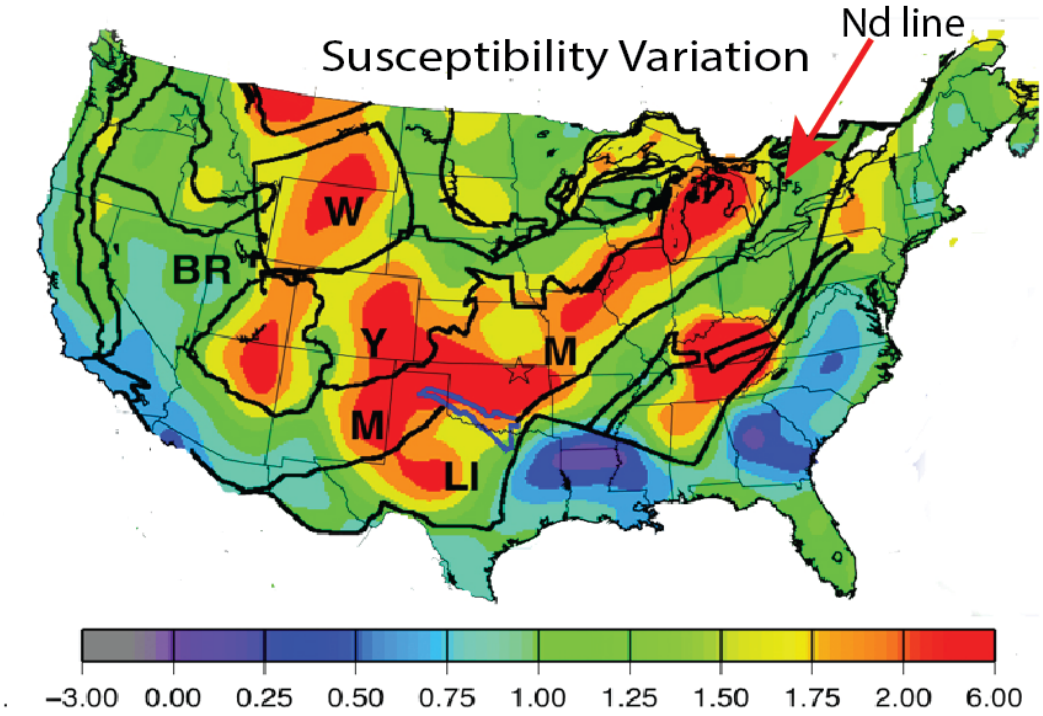

Figure 1.2 Depth-integrated magnetic susceptibility variation from the CHAMP satellite magnetic field model MF7. M-Mazatzal Province, Y-Yavapai Province, W-Wyoming Craton, BR-Basin & Range, Ll-Llano (from Ravat, 2007).

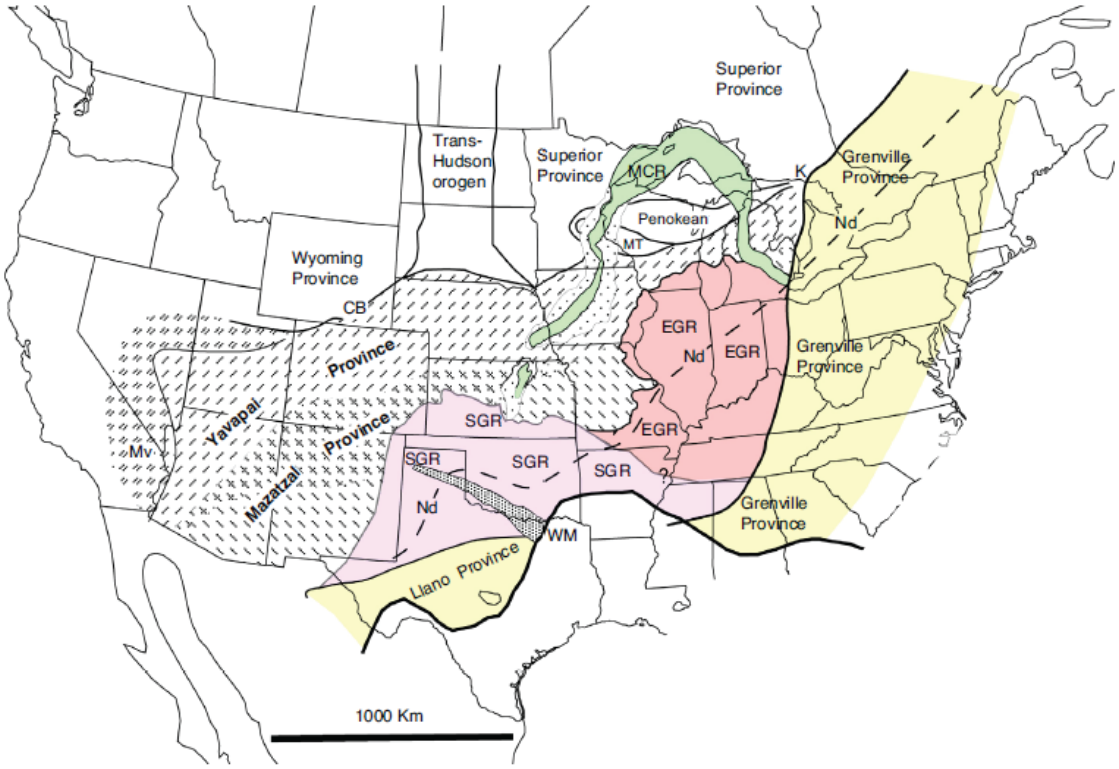

Figure 1.3 Map of the United States illustrating the placement of the Nd mantle derivation age line (dashed line) amongst various Precambrian Laurentian provinces. MCR – Midcontinent Rift, EGR – Eastern Granite-Rhyolite province, SGR – Southern Granite-Rhyolite province, K – Killarney province, MT Marshfield Terrane, WM – Wichita Mountains magmatic province, CB – Cheyenne Belt, Mv – Mojave province (from Bickford et al., 2015).

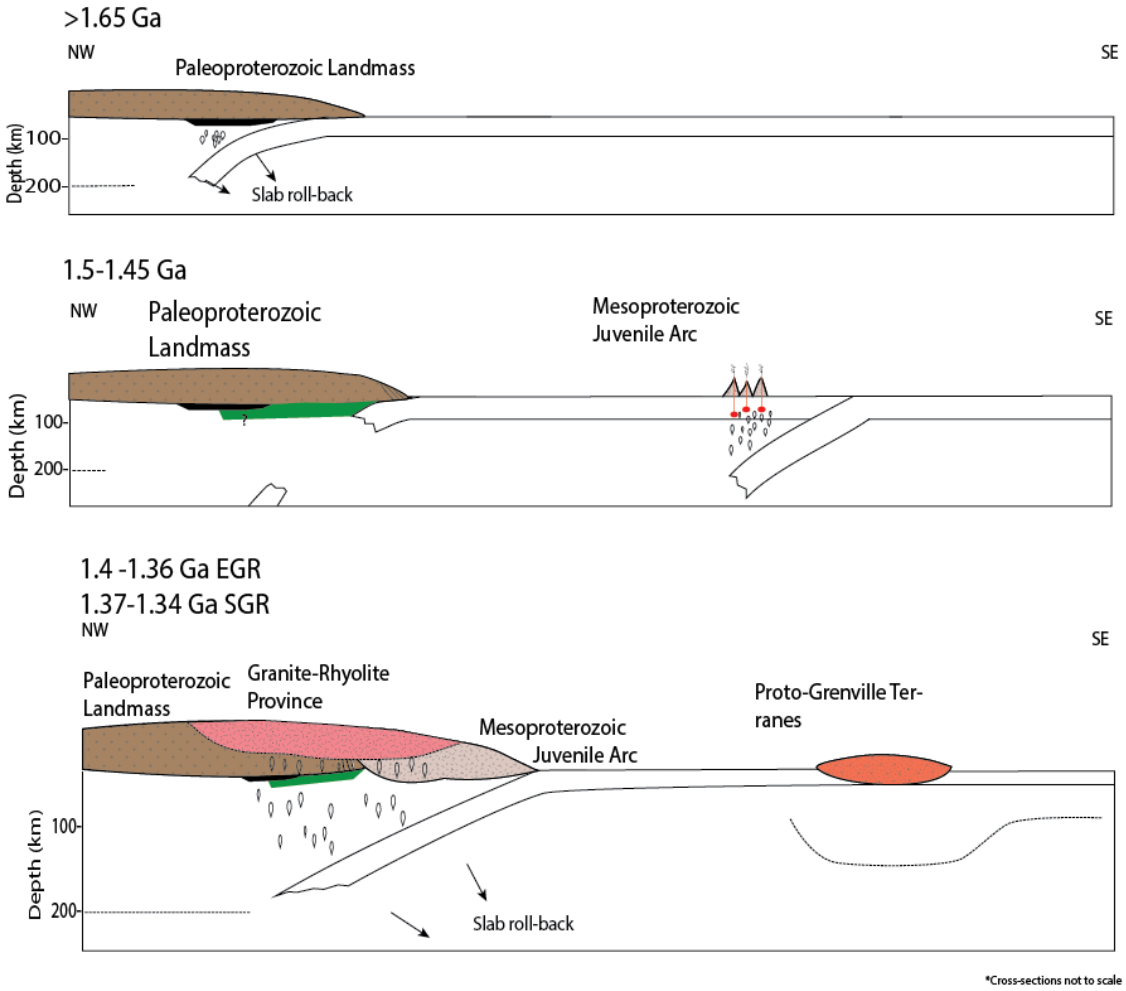

Figure 1.4 Westward-dipping subduction scenario potentially responsible for the formation of zone of high magnetization and Eastern Granite Rhyolite province.

Chapter 2 Background

A. The Archean Laurentian Craton

The history of the Laurentian craton is extensive and complicated by its longevity. With cores from rocks in its western margin ranging in age in excess of 3.5 Ga (Whitmeyer and Karlstrom, 2007) to the relatively recent Grenville Front (1.1 Ga) on the southeastern margin, the successions of continental scale accretion and rifting provide layers of history that need to be considered before investigations in a specific region from a specific time. A topic of intensive research, understanding the history of the amalgamation of Laurentia in the midcontinent has proven to be frustrating at times due to the complexity of the region and limited access to basement samples.

Although Laurentia has undergone significant modification throughout its existence, a large amount of the early history is readily accessible within the interior of the craton. Archean blocks such as the Slave, Rae, Hearne, Wyoming, and Superior, which contributed to the formation of its core in the period spanning roughly 2.5-2.0 Ga and into the early Paleoproterozoic (Hoffman, 1988), are found exposed in various parts of North America and consequently provide direct access to samples from this time period. Reworking of these old Archean cores by subsequent deformation can be determined through sample analysis more readily than their Paleoproterozoic and younger counterparts lying on the southeastern margin. Millions of years of deposition have left these younger terranes covered by a thick layer of sediment deposited in the Paleozoic and Mesozoic; hence, access to the basement and bedrock in these regions is isolated and samples from these regions are not fully representative as a whole due to the sparse coverage.

Suture zones found between reworked Archean blocks (such the Trans-Hudson orogen stitching the Wyoming, Hearn, Medicine Hat, and Superior provinces) illustrate the geologic processes that occurred during the initial formation of the craton (Whitmeyer and Karlstrom, 2007). Subduction-related events are seen throughout much of the Proterozoic on the southeastern and southwestern margins: of prominent interest are the younger Paleoproterozoic Yavapai and Mazatzal terranes, both of which accreted to Laurentia as a result of the collision of arc terranes and other subduction-related activity.

B. The Yavapai and Mazatzal Terranes

The 1.9-1.8 Ga Paleoproterozoic Yavapai province is composed of predominantly juvenile crustal material that accreted as a series of arcs onto the southeastern margin of Laurentia and culminated in the Yavapai orogeny. The remnants of this province span the northern border of the zone of high magnetization in the midcontinent (Figure 1.2). The Yavapai evidences little inherited older material in it as seen through Nd T_{DM} model ages (1.8-2.0 Ga) that are relatively close to the crystallization ages of 1.7-1.8 Ga and thus supports derivation from juvenile accreted material (Bickford et al., 2015). Similar to the Mazatzal, the Yavapai is well exposed in the southwestern United States but remains buried under Paleozoic sediment cover throughout the midcontinent. Although basement access is limited in this region, the province is inferred to be tentatively continuous from the southwest through and into the midcontinent (Whitmeyer and Karlstrom, 2007; Van Schmus et al., 1996, 2007).

The 1.7-1.6 Ga Paleoproterozoic Mazatzal province directly underlies the region of high magnetization (Figure 1.2). Crust formed during this time period was primarily of mafic nature with the oldest rocks consisting of "…volcanogenic greenstone successions… composed of basalt and basaltic andesite…" (Whitmeyer and Karlstrom, 2007). Chemical data for this province is also consistent with an oceanic island arc origin due to the relatively similar nature of T_{DM} model ages and the ages of crystallization. As the province extends northeastward into the midcontinent, a thick layer of sediment was deposited during the Paleozoic, thus obscuring much of the basement in the region. Isolated basement samples for the overlying Eastern Granite Rhyolite (EGR) in the midcontinent have been obtained, however, and Paleoproterozoic T_{DM} model ages far older than the Mesoproterozoic crystallization age were found indicating an older crustal source through which it had to intrude (Nelson and DePaolo, 1985; Bickford et al., 2015). This difference in T_{DM} model ages and ages of crystallization (1.7 Ga vs. 1.5 Ga) provide additional evidence supporting the continuation of the Mazatzal through the midcontinent.

C. The Eastern and Southern Granite Rhyolite Provinces

The primary basement rocks of the midcontinent belong to the Mesoproterozoic Eastern and Southern Granite Rhyolite (EGR and SGR) provinces which formed approximately 1.45-1.3 Ga. Spanning a large portion of the central, southeastern, and southwestern United States (Figure 2.1), the EGR and SGR provinces are composed of massive quantities of granite and rhyolite primarily believed to have an anorogenic formation (Slagstad et al., 2009; Van Schmus et al., 1996). Numerous studies have been done over the years without producing a universally satisfactory answer on their origin. As previously mentioned, the EGR (and the SGR, to a lesser extent) are both covered by sediment, yet because they also cover the deeper basement crust, information on their source rock origin and on this deep basement can be found in the geochemical data extracted from core samples. A difference in both the crystallization and T_{DM} model ages on the northwestern side of the Nd line suggests formation through reworking of older Paleoproterozoic crustal material whereas the southern side of the line illustrates similar T_{DM} model and crystallization ages and consequently a more juvenile mantle source (Bickford et al., 2015; Van Schmus et al., 1996; Van Schmus et al., 2007). Samples taken from the EGR provide these T_{DM} model ages and help define the location of the Nd chemical boundary by delineating the transition of Paleoproterozoic to Mesoproterozoic material. But the crystallization ages from the EGR (~1.45 Ga) and SGR (~1.35 Ga) are 100 million years apart and may imply a diachronous collision along the southeastern margin of Laurentia if these rocks formed by subduction related remelting of the lower crust. This timing pattern is seen in the decreasing crystallization ages from the northeast to the southwest along the Nd line (Bickford et al., 2015; Nelson an DePaolo, 1985; Slagstad et al., 2009; Van Schmus et al., 1996). Because of the juxtaposition of ages on either side of the Nd line, it is a likely candidate to geochemically represent a suture zone between Paleoproterozoic and Mesoproterozoic blocks that collided into one another during the Mesoproterozoic. Numerous small plutons and clusters of granite are also believed to be of anorogenic formation and are widely dispersed throughout both the EGR and SGR (Whitmeyer and Karlstrom, 2007). Due to a lack of constraint on their formation origin however, orogenic sources could also be considered due to the complicated history of southeastern Laurentia (Slagstad et al., 2009).

D. The Nd T_{DM} Model Age Geochemical Separation Line

The Nd T_{DM} model age line (Nd line) was first identified by Van Schmus et al. (1996), but at the time not much was known and the implications of it were not fully recognized until the subsequent decade. The Nd line forms the southeastern border of the zone of high magnetization running through the midcontinent (Figure 1.2). Sm-Nd dating measures the ratio of ^{147}Sm that decays to ^{143}Nd and the ratio $^{143}Nd/^{144}Nd$ which subsequently provides information on both age and provenance of a sample by examining the fractional deviation from bulk earth (ε_{Nd} and ε_{Hf}) (DePaolo and Wasserburg, 1976). Positive ε_{Nd} values are indicative of a more juvenile, mantle-based origin whereas negative values signify derivation from preexisting crust. The aforementioned positive and negative epsilon Nd values are based on the deviation of $^{143}Nd/^{144}Nd$ from bulk earth evolution starting from chondritic uniform reservoir (CHUR) (see DePaolo and Wasserburg, 1976, for a complete description of the dating process). The primary advantage of using Sm-Nd age dating is in the information obtained on provenance and age of mantle derivation. Samples from the southeastern side of the Nd line have greater positive ε_{Nd} values indicative of a younger and more juvenile source whereas the northern side has lesser positive to negative ε_{Nd} values and is believed to originate from an older Paleoproterozoic crustal source (Figure 2.2) (Bickford et al., 2015). Figure 2.2 plots ε_{Nd} values with respect to the corresponding ε_{Hf} values; the line at $\varepsilon_{Nd}=2$ divides the "old crust" from the "young (juvenile) crust" (Bickford et al., 2015). A distribution of samples' ages with respect to their distances from the Nd line is shown in Figure 2.3. The sources in the negative distance region extend into the older cratonic crust whereas the younger sources extend towards a more juvenile crust on the positive side of the x axis (Bickford et al., 2015). Figure 2.4 is a map illustrating the distribution of Nd T_{DM} sample dates with respect to the Nd line (Bickford et al., 2015).

E. Modern Analog to Izu-Bonin-Mariana Arc System

Discussion on the assembly of Laurentia illustrates the complex history of the region. As such, many interpretations exist that attempt to describe its various geologic features. Subduction that reverses polarity has long been a proposed scenario of the southeastern margin used to explain geochemical patterns seen in the midcontinent (Van Schmus et al., 1996). The revised subduction setting (Figure 1.4) provides a tectonic

framework that explains the observed zone of high magnetization while simultaneously explaining the formation of the EGR. Plate roll-back accounts for the massive flood of granite and rhyolite while also providing a mechanism for metasomatization of the crust and the production of titanomagnetite and magnetite. A modern analog for this setting is seen in the Izu-Bonin-Mariana Arc system in the western Pacific. Intra-oceanic subduction on the eastern margin of the Philippine Sea and extension due to rapid convergence rates on the western margin of the Philippine Sea plate produces chains of islands arcs that will subsequently end up accreting onto larger landmasses in the west (Hawkins et al., 1984; Stern et al., 2013). In this setting, islands arcs created in the system are representative of the formation of the Mazatzal province that then accreted onto the southern margin of Laurentia. Island arc material is primarily characterized by the calc-alkaline suite of magmatic rocks (Green and Ringwood, 1968; Percival and Mortensen, 2002), material that has been found in plutons of the American southwest within the Mazatzal province (Whitmeyer and Karlstrom, 2007).

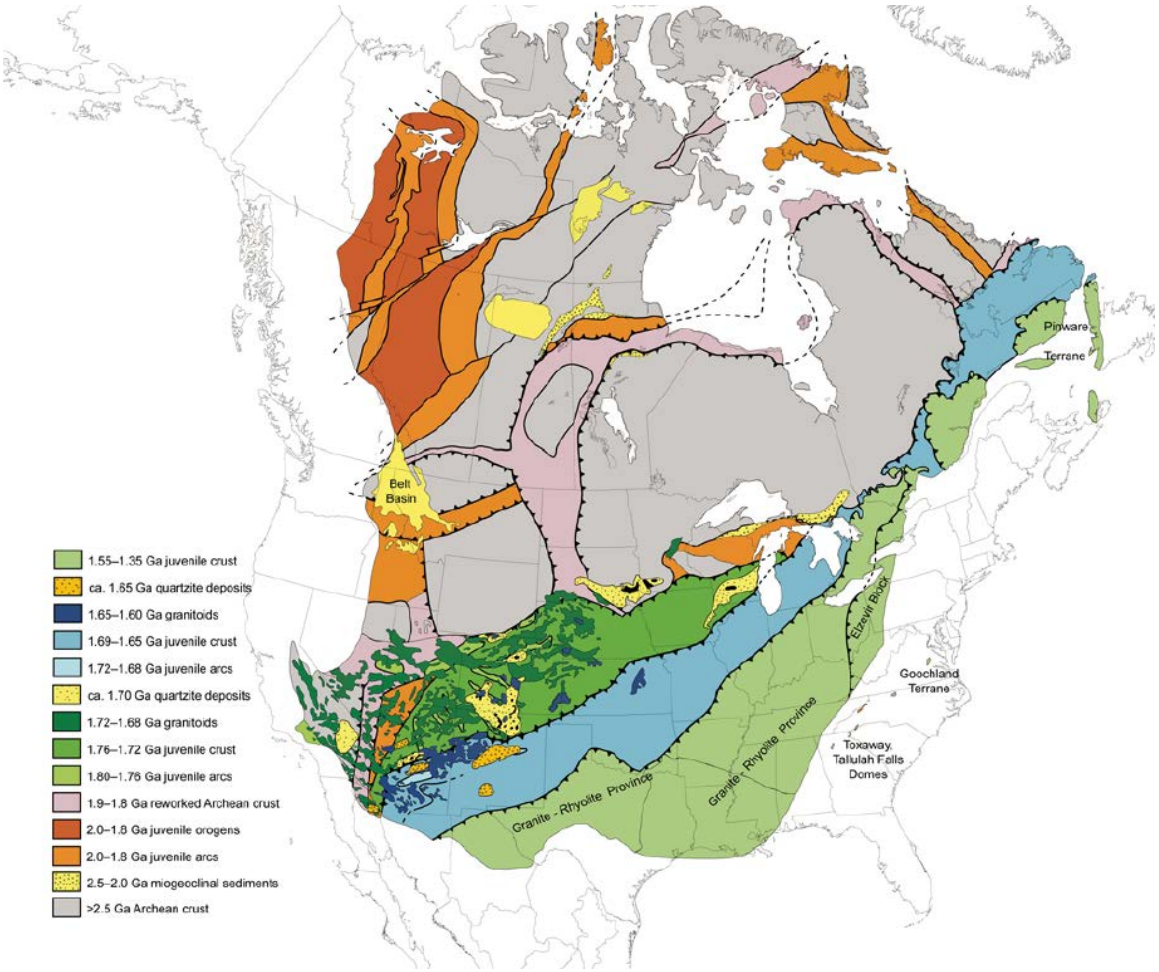

Figure 2.1 Position of the Paleoproterozoic Yavapai and Mazatzal provinces in addition to the Mesoproterozoic Granite Rhyolite provinces against the older Archean blocks illustrating continental growth (from Whitmeyer and Karlstrom, 2007).

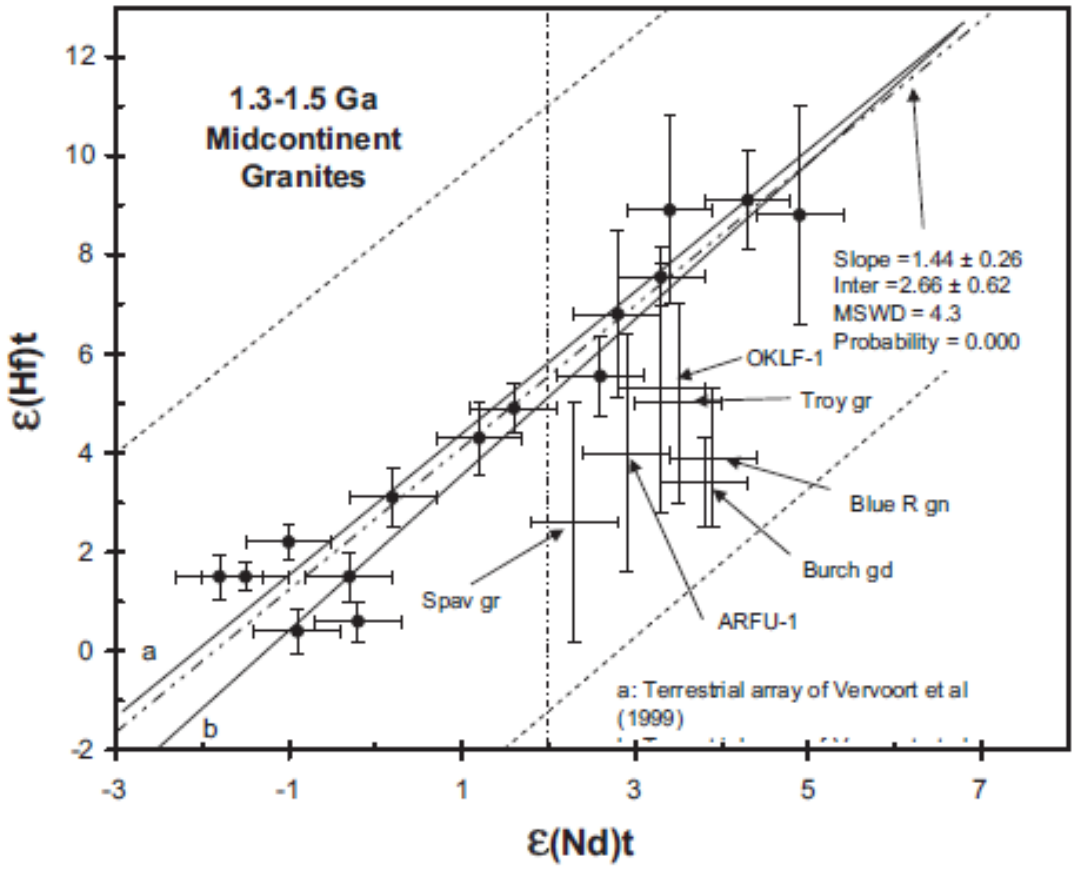

Figure 2.2 Plot of ε_{Nd} vs. ε_{Hf} for the same samples from Figure 2.4 and Figure 2.3. Dividing line at ε_{Nd}=2 separates the higher ε_{Nd} and ε_{Hf} values that suggest juvenile crust from the lower and negative ε_{Nd} and ε_{Hf} values that indicate older crust (Bickford et al., 2015).

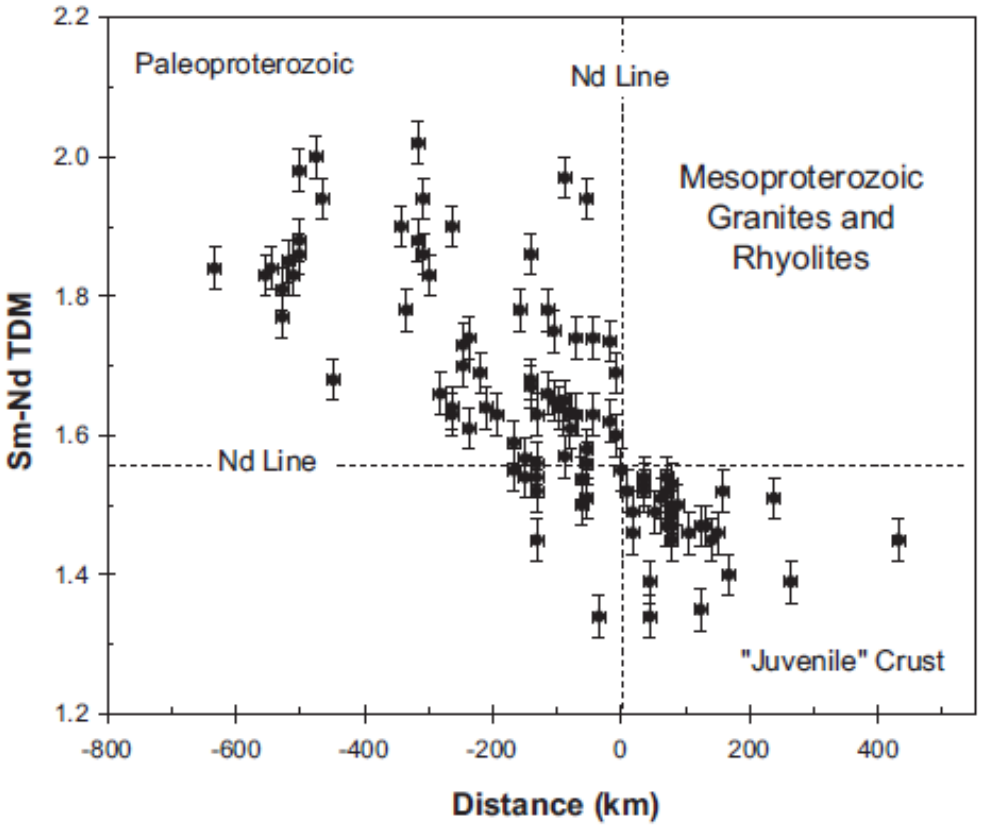

Figure 2.3 Nd T_{DM} model age versus distance from the Nd line. Negative distances are measured into the older craton and positive distances are measured into the juvenile crust southeast of the Nd line (from Bickford et al., 2015).

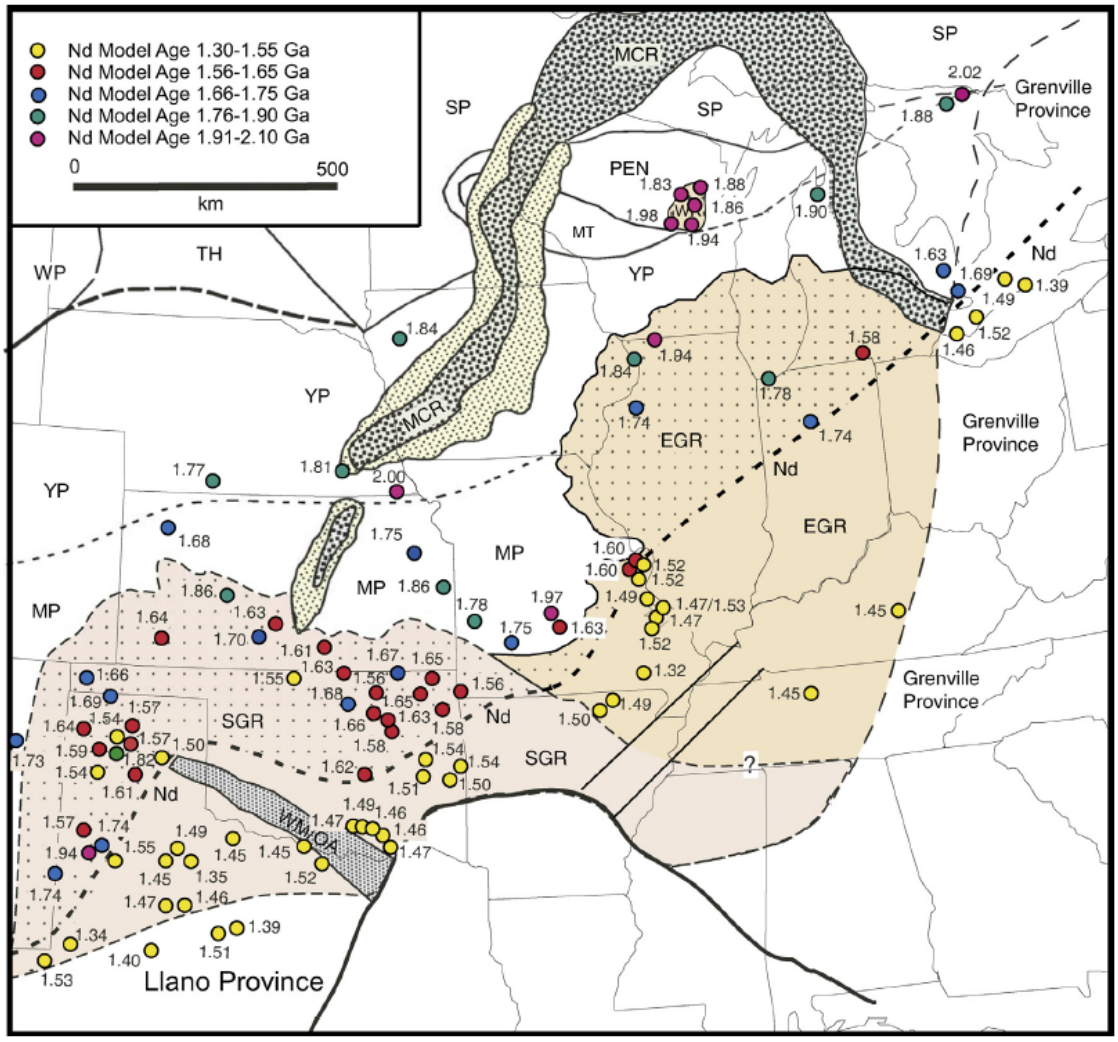

Figure 2.4 Nd model age data in the midcontinent illustrating the dichotomy of ages as seen in the Paleoproterozoic to the north of the T_{DM} line and Mesoproterozoic to the south (from Bickford et al., 2015).

Chapter 3 Geophysical Modeling

A. Long Wavelength-Corrected Magnetic Anomaly Datasets

The NURE_NAMAM2008 aeromagnetic dataset (Ravat et al., 2009) (Figure 3.1) was used to create the primary total intensity magnetic anomaly grids because long-wavelength anomaly fields which arise from the deeper magnetic sources of interest in this study are preserved accurately in this dataset. This is accomplished by correction of long-wavelengths in the United States lower 48 states using reprocessed NURE (National Uranium Reconnaissance and Evaluation) 2° longitude x 1° latitude surveys with the continuous core field model CM4 (Sabaka et al., 2004). The rest of the map contains the same database as the North American Magnetic Anomaly Map of 2002 (Bankey et al., 2002). The original NURE data were collected during the 1970s as a series of aeromagnetic surveys over the continental United States in an effort to determine resource potential of uranium, thorium, and potassium and other natural resources and it provided one of the first magnetic field datasets covering the entire United States. The NURE data were corrected originally using International Geomagnetic Reference Field (IGRF) core field. The IGRF/DGRF (D for definitive) which represent the Earth's core field in the magnetic observations are compiled from five year's worldwide geomagnetic observatories, repeat stations, and satellite and other magnetic survey datasets and they tend to represent inadequately and discontinuously the core magnetic field when global coverage of satellites is not available. This was the case in the 1970s when NURE surveys were flown and thus the differences in survey parameters, primarily time of measurements, led to edge discontinuities. Additional constraint of continuity through time and space from the Comprehensive Model 4 (CM4) allows determination of the core field more accurately and also permits isolation of long-wavelength ionospheric and magnetospheric fields and thus reduces base level shifts between surveys while also maintaining the long wavelength magnetic anomalies within the dataset (Ravat et al., 2009). This map, in the continental United States excluding Alaska, has wavelengths > 50 km from CM4 processing of NURE surveys and the rest is same as NAMAM2002 compilation. This is accomplished through removal of the main field component from the crustal field based on the CM4 model.

The total intensity magnetic anomaly field is computed by subtracting the time-varying core field, **F,** from the measured total field corrected for the diurnal field variation. This total field magnetic anomaly T is given by

$$T = \boldsymbol{F} + \Delta T \tag{1}$$

where ΔT is the perturbation resulting from an anomalous magnetic source (Blakely, 1995). The total intensity T is a scalar quantity that can be described using the three directional magnetic field components in the Cartesian coordinate system as a square root of sum of squares (Blakely, 2005).

$$T = \sqrt{F_x^2 + F_y^2 + F_z^2} \tag{2}$$

In order to produce the combined NURE_NAMAM2008 dataset, CM4 was subtracted from total intensity T to remove the main field component from the dataset.

$$\Delta T = \sqrt{F_x^2 + F_y^2 + F_z^2} - \sqrt{F_{CMx}^2 + F_{CMy}^2 + F_{CMz}^2} \tag{3}$$

Additionally of importance to the modeling and interpretation are magnetic inclination and declination. The magnetic inclination, I, defines the vertical angle between the magnetic field vector and the horizontal plane (Blakely, 1995) and thus

$$I = arctan\left(\frac{F_z}{\sqrt{F_x^2+F_y^2}}\right) \tag{4}$$

and magnetic declination, D, the azimuthal angle of the vertical plane which contains the magnetic field vector w.r.t. geographic north (Blakely, 1995) such that

$$D = arcsin\left(\frac{F_y}{\sqrt{F_x^2+F_y^2}}\right) \tag{5}$$

In the local magnetic coordinate system, x is northward, y is eastward and z is downward. The North American Magnetic Anomaly Map (NAMAM) was created for geophysical exploration. The highs and lows of total intensity magnetic anomalies do not always correspond to geochemically-defined geological provinces (Figure 3.2). At non-vertical inclinations, anomaly peaks and troughs are displaced with respect to their sources. The total intensity magnetic anomalies also retain the effect of remanence associated with magnetic sources that could potentially skew the correlation of the magnetic boundaries

with geologic and geochemically defined province boundaries. At the same time, however, the total intensity magnetic anomalies allow modeling of any potential remanent crustal sources that would be undetected or misinterpreted in a reduced to pole (RTP) dataset. Even though the magnetic field changes are displaced with respect to their sources and do not exactly correlate with the geochemical boundaries, the larger trends are still as apparent as in the depth integrated magnetic susceptibility map where the process of converting anomalies to susceptibilities remove these effects (Figure 1.2).

The primary software used for modeling and data management is Geosoft Oasis Montaj. Oasis Montaj provides a platform for housing multiple large datasets and offers tools for additional manipulation such as filtering, modeling and interpretation. In order to create the long wavelength magnetic anomaly grids, NURE_NAMAM2008 was imported into Oasis Montaj. Because the zone of high magnetization is only visible in the long-wavelength spectrum, it requires additional filtering to remove the near surface short wavelength sources that normally obscures it. This processing is done with the MAGMAP module using fast Fourier transform (FFT) of the total intensity anomaly grid. Fourier transform are advantageous for filtering as they can alter both periodic and aperiodic functions with the latter being applicable to both gravity and magnetic data. Filtering removes undesirable noise or signal in order to examine specific features of a dataset – in the case of this study, long-wavelength magnetic anomalies are retained so that they could be independently modeled in addition to total field anomalies. For a function of two directional variables, $f(x, y)$, the relevant Fourier and inverse Fourier transforms, respectively, are

$$F(k_{x,}k_y) = \iint_{-\infty}^{\infty} f(x,y)e^{-i(k_x+k_y y)}dxdy \tag{6}$$

$$f(x,y) = \frac{1}{4\pi^2}\iint_{-\infty}^{\infty} F(k_{x,}k_y)e^{i(k_x+k_y y)}dk_x dk_y \tag{7}$$

where $k_x = \frac{2\pi}{\lambda_x}$ and $k_y = \frac{2\pi}{\lambda_y}$ (Blakely, 1995). Here, k_x and k_y are the wavenumbers in the x and y directions and λ_x and λ_y are the wavelengths in the x and y directions. Continuing, the Butterworth low pass filter expression in Geosoft Oasis Montaj is

$$L(k_x, k_y) = \frac{1}{\left[1+\left(\frac{\sqrt{{k_x}^2+{k_y}^2}}{k_c}\right)^n\right]} \tag{8}$$

where n is the "positive integer value determining the degree of sharpness of the cutoff", and k_c is the "inflection point of wavenumber cutoff in cycles/ground unit." The Butterworth filter coefficients $L(k_x, k_y)$ are multiplied with $F(k_x, k_y)$ and then inverse transformed to obtain the filtered anomalies. The NURE_NAMAM2008 dataset was gridded at 1.25 km spacing and subsequently Butterworth low-pass filtered at 100, 200, 300, and 400 km. Low pass filtering was used on the NURE_NAMAM2008 aeromagnetic data in order to approximate the long-wavelength magnetic anomalies seen from the CHAMP satellite data. Because the high magnetization anomaly seen in the depth-integrated magnetic susceptibility map (Figure 1.2) is best observed in the 300 km low-pass anomaly, the corresponding low-pass filtered grid was used for the purpose of illustration and the boundaries of the Yavapai, Mazatzal, Eastern Granite-Rhyolite (EGR), and Nd line were placed on the maps (Figure 3.2). Profiles perpendicular to the Nd line that bisect multiple provinces were selected from the magnetic anomaly and other relevant datasets to forward model the region of high magnetization.

B. Additional Datasets

Additional datasets important for modeling include the complete Bouguer gravity anomaly data compiled from Pan-American Center for Earth and Environmental Studies (PACES) at the University of Texas at El Paso (UTEP) for the United States, supplemented by WGM2012 (Figure 3.3) (H. L. Zhang, 2017, pers. comm.); the sedimentary thickness data from Chulick and Mooney (2002) merged with the Illinois basin data of Ellett and Naylor (2016) by H. L. Zhang (2017, pers. comm.) (Figure 3.4); topography (Figure 3.5) (USGS Topo Map Collection); the depth to the Moho (Figure 3.6) (A.R. Lowry, 2016, pers. comm.); and the depth to base of magnetization to constrain the depth extent of magnetic sources contributing to the overall regional anomalies (D. Ravat, 2017, pers. comm.; Figure 3.7). All datasets were gridded at 1.25 km spacing in the DNAG projection in order to match NURE_NAMAM2008 and facilitate accurate extraction of information from supporting datasets through Geosoft Oasis Montaj. Depth to the base of magnetization is derived through spectral analysis of magnetic anomalies using the de-fractal method (Figure 3.7) (see Ravat et al., 2016, and

Salem et al., 2014, for a complete description of the method). Uncertainties and margins of error for all datasets are displayed in Table 3.1.

C. 2D Potential Field Modeling

The Paleoproterozoic zone of high magnetization was modeled at three different profile locations along the Nd geochemical boundary. In order to create the models, Geosoft Oasis Montaj and its integrated GM-SYS modeling program provide platforms to incorporate datasets and build the 2D models. GM-SYS creates block and polygon models that can be constrained by geologic knowledge of the region and available datasets (sedimentary thickness, depth to the base of magnetization, and depth to the Moho). Data along each profile can be extracted from these datasets and provide the initial horizons around which the model is built. Data extracted from grids for each modeled profile is collected into a single database which can be imported into the modeling program. Total intensity long-wavelength-corrected aeromagnetic data (hereafter NURE_NAMAM2008 magnetic anomalies were imported and subsequently Butterworth low-pass filtered as previously mentioned. The primary advantage of using a Butterworth filter as opposed to a standard low-pass is that it is has prescribed tapers with known characteristics to avoid ringing artifacts caused by Gibb's phenomenon at the edges of the filter. As the high intensity anomaly zone is only visible in long-wavelength magnetic data, multiple grids at various low-pass cutoff filters allow more careful examination of the boundaries of the anomaly and provide an insight into how the anomalies from neighboring zones of high magnetization coalesce into the observed anomaly high. These filtered magnetic anomaly maps were compared with the depth-integrated magnetic susceptibility maps to further constrain the zone of interest.

Geochemically-defined geologic maps (Figure 1.3; Figure 2.1; Figure 2.2) were consulted in order to provide rock type constraints for the crystalline basement and the upper crust. All three profiles cross through the Granite-Rhyolite (Figure 3.2) and the depth extent of this province was set to average upper crustal thickness of 10 km (Rudnick and Fountain, 1995). Using the layering from the constraining datasets (sedimentary depth, topography, depth to the Moho, depth to base of magnetization), simple magnetized blocks were created to match the observed 100 km filtered (Figure 3.8) anomaly data (Figures 4.8 and 4.9) through visual inspection. The upper crust is

brought from the base of sediments to 10 km depth, the middle crust from 10 km to 26 km, and the lower crust from 26 km to the Moho. In some instances, a sub-lower crustal layer was constructed between the lower crust and the mantle (from ~40 km to the Moho) in order to facilitate greater densities at greater pressure near the deep base of the crust (Gebrande, 1982). In the total intensity magnetic profile, there are a number of short-wavelength high amplitude features and, except in a few areas of subdued anomalies, it is difficult to observe relative high and low magnetization deeper sources. The 100 km low-pass was used initially to build the regional magnetic variations. Within the 100 km low-pass anomaly grid, the outline of the zone of high magnetization is definable while maintaining amplitudes closer to the total intensity anomaly profile than the 300 km low-pass provides. Once the calculated anomaly approximately matched the 100 km low-pass filtered observed anomaly, the total intensity magnetic anomaly data were used to add small, near-surface sources in primarily the upper crust to match the short wavelength higher anomaly amplitudes. Magnetic and gravity parameters of the models were modified until the calculated total intensity matched the corresponding observed anomalies. Physical property ranges for the rocks expected in the region (Paleo and Mesoproterozoic, Granite-Rhyolite, and Grenville provinces) were taken into account during the modeling (Hinze et al., 2013).

As discussed earlier, three profiles were modeled orthogonal to the zone of high magnetization. A southern profile in Illinois crosses a zone of relatively intermediate intensity, the second through a quieter zone in the region of high magnetization to serve as a reference profile, and third taken at the far northern edge of the magnetic anomaly and Nd chemical age boundary (T_{DM}) in the Great Lakes region extending from Virginia to Lake Superior (Figure 3.2). Each profile is modeled independently of the others and then the three are analyzed for similarities and differences in the magnetic values used to simulate the observed magnetic anomalies. Earth field parameters, required for determining regional magnetic inclination and declination, were set at the location where each profile crosses the T_{DM} line, approximated by the southern boundary of the Mazatzal province (Whitmeyer and Karlstrom, 2007). The models are colored according to geologic/age provinces of Whitmeyer and Karlstrom (2007) and Bickford et al. (2015).

The profiles were named “ND_SW” (the southwesternmost profile in Figure 3.2); “ND_REFERENCE” (the middle) and “ND_NE” (the northeasternmost).

C1. 2D Magnetic Modeling of Profile ND_REFERENCE

Profile ND_REFERENCE is the middle of the three in Figure 3.2. The profile samples the lowest amplitude region of the zone of high magnetization among the three profiles. The first 2D model created from this profile models the 100 km low-pass anomaly (Figure 3.9). The magnitude of the magnetic field intensity in this region is 56,400 nT with an inclination of 70º and declination of -4º. These values are representative of the region modeled in this profile. Since the base of magnetization in the region is 20-25 km, the purpose of this model is to illustrate that the middle crustal zone of high magnetization sources can lead to the large long-wavelength magnetic anomaly that was inferred from the satellite based magnetic models. In Figure 3.9, the uppermost crystalline crust was given a susceptibility value of 0.01 SI. In the Paleoproterozoic zone of high magnetization, susceptibility values range from 0.02 SI to 0.09 SI. These fall within the observed range of values for dioritic and (on the high end) gabbroic material (Clark and Emerson, 1991; Clark, 1997; Clark, 1999). The heat flow in the region is low (~50 mW/m^2) and, based on geothermal modeling, it leads to temperatures of 200°-300°C at the depth where the base of crustal magnetization is located (D. Ravat, 2017, pers. comm., Figure 3.10). This range of Curie temperature is consistent with titanomagnetites and titanohematite of intermediate composition of these solid solution series. Heat flow is an important parameter to consider for the spectral depth to the base of magnetization determinations as this limits to extent of magnetized crust. Modeled susceptibilities are highest on the northwestern side of the T_{DM} line with an average of 0.04 SI for the Paleoproterozoic Mazatzal and 0.07 SI for the early Paleoproterozoic Superior, Yavapai, and Penokean terranes northwest of the Mazatzal. Values for upper crustal intrusions range from 0.01 SI to 0.07 SI. All susceptibilities used here lie within the range of observed values for I-type granites (Clark and Emerson, 1991; Clark, 1997; Clark, 1999).

Several strong magnetic lows along the profile require very low susceptibilities (less than 0.005 SI) and remanent magnetization could be responsible for these (570 km and 660 km, 3.5 km to 10 km depth, Figure 3.12). By examining the total intensity

magnetic anomaly map, orientation of observed anomaly highs and lows in relation to the present day field can provide information on whether or not remanence could exist. Present day inclination in the region will lead to a magnetic low to the north and a high to the south of the source body. The two previously mentioned magnetic anomaly lows modeled in Figure 3.11 were candidates for remanent magnetization due to the intensity of the anomalies. No clear magnetic dipolar features were located along the profile, however, and remanence opposite to the present day field orientation was used due to the lack of guidance from observed anomalies. The modeled results were consistent with the observed total intensity magnetic anomaly when this remanence was applied. Remanent magnetization was not included in the long-wavelength models. In Figure 3.11, the blocks containing remanent magnetization are centered at 570 km and 660 km and have magnetization values of 1.4 A/m and 2.5 A/m and an apparent inclination and declination of -45º and 200º, respectively.

Several geologic features are apparent in the total intensity profile. The large gravity low in the northwest (14 km to 190 km, modeled from surface to 10 km depth with intrusions, Figure 3.11) is created by the Wolf River Batholith (WRB) intruded into early Paleoproterozoic and reworked Archean basement (previously modeled by Allen and Hinze, 1992). Models from this study and Allen and Hinze (1992) agree on low density values necessary to produce the observed anomaly, all less than 2800 kg/m^3. The wide range of susceptibility values (less than 0.001 SI and up to 0.06 SI) measured by Allen (1990) for the WRB also agree with those used in this model; the susceptibilities of the upper crustal blocks are set at 0.01 SI for both ND_REFERENCE total intensity and 100 km low-pass anomalies. Several differences in physical properties and variations of layers of provinces or orogenies are observed in the models. The Grenville region has a deeper Moho than the Mesoproterozoic crust to its northwest.

C2. 2D Magnetic Modeling of Profile ND_SW

The ND_SW was chosen because it samples the middle of the NE-SW trending Mazatzal Province and Nd chemical boundary. It is the southwesternmost profile on Figure 3.2. The profile extends from Archean aged terranes in the northwest to the Neoproterozoic Grenville front in northern Georgia along an azimuth of 138.26º. Magnetic field parameters were set at the location 88ºW38ºN. The magnitude of the

magnetic field intensity in this region is 55,100 nT with an inclination of 68º and declination of -0.7º. The profile crosses the Illinois sedimentary basin. Because of the extensive depth of sediments in the region, basement core samples are scarce (Bickford et al., 2015). Limited exposures surrounding the region, such as in the St. Francois Mountains of Missouri, provide data to constrain the location of the T_{DM} chemical boundary (Bickford et al., 2015; Rohs and Van Schmus, 2007; Van Schmus et al., 1996). The location of the T_{DM} age line (i.e., the southeastern edge of the Mazatzal province) of Van Schmus et al. (1996) roughly corresponds to the southeastern boundary of the Mazatzal province defined by Whitmeyer and Karlstrom (2007); the latter was used in this study because a digitized version of it is available.

The 2D profile of ND_SW with accompanying potential field data is shown in Figure 3.12. The depth extent of the upper crustal granitic rocks of the EGR province has been previously inferred to be around 10 km from the surface in Ohio (Lucius and von Freese, 1988; Whitmeyer and Karlstrom, 2007). The areal extent of the EGR used in the model is derived from Bickford et al. (2015), as they have provided updated geochemical data and redefined Paleoproterozoic province boundaries. All Proterozoic boundaries in the models were derived from Bickford et al. (2015), and cross-checked with those from Whitmeyer and Karlstrom (2007). The model shows a deep sedimentary basin (the Illinois Basin) (Figures 3.4 and 3.12, 860-1180 km, >4 km depth) and a locally elevated Moho and thickened middle crust (Figure 3.6) (Figure 3.12, 860-1180 km, the Moho at 46 km depth). The depth to the base of magnetization also follows the trace of the Moho. Finally, a small triangular feature in the deep part of the sedimentary basin is seen mimicked in the upper crustal magmatic intrusions (Figure 3.12, 998 km, 4 km depth). The magnetic high is significantly more prominent than the gravity, but both are likely related to this feature.

Figure 3.13 illustrates the first of two mantle scenarios that could contribute magnetization to the anomaly. Underplating is a mechanism in subduction settings where gabbroic magma may pond beneath and adheres to the lower crust in the mantle (Thybo and Artemieva, 2013). Depth to the base of magnetization sets the lowest limit of magnetite/titanomagnetite, the primary high susceptibility mineral in the crust, between 20 and 40 km (Figure 3.12); however, spectral windows of the order of 1000 km and heat

flow modeling suggests that deeper magnetization (up to 60 km) may be possible (D. Ravat, 2017, pers. comm.; Figures 3.10 and 3.13). While underplating has the potential to contribute magnetization to the base of the crust, the gravity anomaly created by the less dense material (3000 kg/m^3 for gabbroic material as opposed to 3300 kg/m^3 for mantle peridotite) in the mantle causes a large gravity low (~ 75 mGal) that is difficult to reconcile with the observed anomaly (Figure 3.12).

Figure 3.14 shows the second mantle magnetization scenario. Serpentinization of the forearc mantle is believed to be an ongoing process observed in the Pacific Northwest where the Juan de Fuca slab subducts beneath the North American Plate (Blakely, 2005). The process involves metasomatization of mantle peridotite from the hydrated subducting oceanic slab. As the slab heats up, it dehydrates and transfers water to the forearc mantle above it, thus causing melting and the formation of magnetite from the serpentinite created from hydration of peridotite (Hyndman and Peacock, 2003). Potential field modeling of a hypothetical serpentinized wedge (Blakely, 2005) shows that there should be a magnetic anomaly high caused by the serpentinized material along with a gravity low due to its lesser density relative to mantle peridotite. The primary drawback to applying this scenario to the Paleoproterozoic terrane is age. Assuming the region was once-serpentinized during the Paleoproterozoic, the serpentinite would eventually revert back into mantle peridotite after subduction/hydration ends; however, the magnetite created during serpentinization would remain magnetite and it will be magnetic if temperatures in the uppermost mantle (approximately the top 10-15 km) remain below its Curie point of 580º C.

C3. 2D Magnetic Modeling of Profile ND_NE

The final profile modeled lies the furthest northeast on Figure 3.2. It samples a complex region comprising Grenville in the southeast, Granite-Rhyolite, Paleoproterozoic, the Archean Superior block, and a small region of the Midcontinent Rift, along an azimuth of 136.7º. Earth field parameters were set at the location 83ºW44ºN and calculated main field magnitude of 57,500 nT, 72º inclination, and -7º declination. The Midcontinent Rift (MCR) proved to be a complicating factor in this profile due to the highly magnetic and dense nature of the basaltic material close to the surface and also because the profile runs parallel to the rift in this region. Consequently,

the profile was modeled with the MCR to maintain anomaly levels but the section has been clipped (Figure 3.15) to eliminate a source of complication unrelated to the primary object of the study. While slightly larger average susceptibility was required to match the total intensity Paleoproterozoic anomaly for ND_NE profile than the total intensity profile ND_REFERENCE (0.07 SI opposed to 0.04 SI) in the middle crust; upper crustal intrusions remained at the same maximum value of 0.07 SI, the highest observed susceptibility value for granite (Clark and Emerson, 1991; Clark, 1997; Clark, 1999). The susceptibilities of ND_NE follow the general trend of the southernmost profile: high susceptibilities under the northwestern Archean and Paleoproterozoic side of the T_{DM} age boundary; a quiet magnetic region where the Paleoproterozoic-derived Mazatzal and overlying Granite-Rhyolite provinces cross the Mesoproterozoic (T_{DM}) Granite-Rhyolite; finally, an increase in susceptibility under the younger Mesoproterozoic and Neoproterozoic terranes (Figure 3.15). The highest susceptibility values in the middle crust were found on the Archean and Paleoproterozoic side of the T_{DM} line. Neither mantle magnetization scenario was modeled in this profile due to the initial results from ND_SW showing either the conceptual or modeling difficulties of having sources in the mantle.

Upwarp of the Moho (Figure 3.15, 950 km, 42 km depth) may illustrate isostatic adjustments in response to the deep sedimentary basin formed by the Rome Trough above it (Figure 3.4, 80ºW40ºN; Figure 3.15, 950 km, 5 km depth). It is interesting that the Moho data from ND_SW also shows such upwarp under the sedimentary basin (Figure 3.12, 1060 km, 4 km depth) and, thus, reflects the processes of isostatic adjustments in the lower crust in these sedimentary basins. Within the Rome Trough region, a localized magnetic high is accompanied by a corresponding gravity high. Beneath the zone of high magnetization, a significant Moho uplift (approximately 9 km amplitude) spans the full extent of the modeled anomaly (Figure 3.15, 196-478 km, 37 km depth). An uplifted depth to base of magnetization overlies this feature (Figure 3.15, 350 km, 30 km depth).

D. Gravity Modeling and Inversion

The gravity profiles are derived from the same models used to create the magnetic profiles. As the gravity anomalies have fewer short-wavelength, high-amplitude

variations than the magnetics, fewer blocks were needed to approximate the observed gravity.

To better match the calculated anomalies to the observed, an inversion tool native to GM-SYS was used. Inversion works oppositely to forward modeling. In general, the problem of finding physical properties given the source geometry is linear whereas finding the coordinates of a potential fields source body is non-linear and solved iteratively (Blakely, 1996, Hinze et al., 2013). It takes a given framework, in this case the block model created for the magnetic and gravity anomaly profiles, and changes the densities of the freed parameters (density of the blocks) to fit the observed gravity anomaly. GM-SYS allows up to 100 parameters to vary for alteration at one time. For the purposes of these models, only middle, upper crustal, and upper crustal intrusion densities were freed for inversion. Upper crustal intrusion densities were only freed when short wavelength adjustments were required to fit the small discrepancies in the observed and computed gravity anomaly. Multiple iterations are required due to the determination process. In GM-SYS, the density inversion is also handled in a non-linear manner because one can choose to free up either physical property or body coordinates for a particular iteration. In a non-linear potential fields inversion, it is desirable to have a starting model close to the final configuration in order to achieve the global minimum of the misfit function. Keeping this in mind, a reasonable density model based on all other available constraints (e.g., sedimentary thickness, the Moho depth, etc.) was developed before allowing inversion to find the misfit minimum.

Density inversion was performed on all three profiles. It provided the simplest tool to match the calculated gravity to the observed since constraints on the variation of sedimentary thickness and crustal thickness/Moho are available. All gravity profiles were originally modified by hand to match as well as possible; however, the density inversion made it easier to fit the modeled profile to the observed one. User oversight is necessary and was used to check that these values indeed vary logically horizontally and in depth from block to block. For the ND_SW profile, densities of the serpentinized wedge and mafic underplating were set at their expected values (3300 kg/m^3 and 3000 kg/m^3, respectively) (Clark and Emerson, 1991; Clark, 1997; Clark, 1999; Hunt et al., 1995). Inversion was not used for magnetic susceptibility because more control over

these values was needed since they form the core work of the study. GM-SYS also has the tendency to create unrealistic values when matching anomalies if the starting block configuration is not close.

E. Summary of Modeling Results

Susceptibility values ranged from 0.001 to 0.1 SI for middle crustal blocks. Lesser values of 0.001 to 0.03 SI were needed for the upper crust. While on the high end for granites and diorites, middle crustal values fall within the observed values for both rock types (Clark and Emerson, 1991; Clark, 1997; Clark, 1999). Dioritic values were more applicable to the middle crust due to increasingly mafic nature with depth.

The middle reference profile ND_REFERENCE required the lowest values in the Paleoproterozoic domain to model the profile (0.001 to 0.09 SI for the middle crust), as would be expected of a profile lying in a relatively quiet region of the study zone. The southernmost profile ND_SW required middle crustal values from 0.001 to 0.1 SI in the Paleoproterozoic T_{DM} Mazatzal region as did the northernmost profile ND_NE. Upper crustal igneous intrusions for Paleoproterozoic, Mesoproterozoic, and Grenville regions on all three profiles have susceptibilities from 0.01 to 0.07 SI, values within the observed range for granites (Clark and Emerson, 1991; Clark, 1997; Clark, 1999). Granitic values were used for upper crustal intrusions as it is a likely rock to be found at the top of crystalline basement due to fractional crystallization from melting of the middle and lower crust. In order to replicate the observed magnetic total intensity anomaly amplitudes, upper crustal intrusions were brought from the base of the upper crust to near the top of crystalline basement. For some cases, such as the Paleoproterozoic (T_{DM}) Mazatzal on profile ND_NE (200 km to 500 km, Figure 3.15), the maximum value for granite (0.07 SI) is not enough to match the peak total intensity amplitude. Thus, these intrusions could extend into the sedimentary layer from crystalline basement as the sedimentary thicknesses in this region are based on 1°x1° grid of Laske et al. (2012). However, the blocks underlying the region where maximum values were not enough to match the observed amplitudes were part of a region with smaller total magnetizable thickness than the other regions.

An uplifted Moho exists in several places on all profiles in the regions of deep sedimentary basins. These deep basins fill with low density sediments over time causing

a negative lateral density contrast with surrounding high density crystalline rocks. The Moho compensates for this density contrast by uplifting under the basin to bring the region back into semi-isostatic equilibrium (200 km to 500 km, 800km to 1100 km, Figure 3.15).

Table 3.1 Estimated resolution of and margins of error for datasets used in creation of the models. NURE_NAMAM2008 (D. Ravat, 2017, pers. comm.); CBA Gravity (H.L. Zhang, 2017, pers. comm.); Depth to Base of Magnetization (D. Ravat, 2017, pers. comm.); Sedimentary Depth (Laske et al., 2012); Depth to the Moho (Chulick and Mooney, 2002).

Dataset	Spatial Resolution	Margin of Error
NURE_NAMAM2008 Aeromagnetic Data	1.25 km	+/- 1-5 nT
CBA Gravity	2-5 km	+/- 0.05-0.1 mGal
Depth to Base of Magnetization	125 km	+/- 10% of depth
Sedimentary Depth	1º x 1º grid	+/- 10 m – 2 km
Depth to the Moho	70 km	+/- 10% of depth

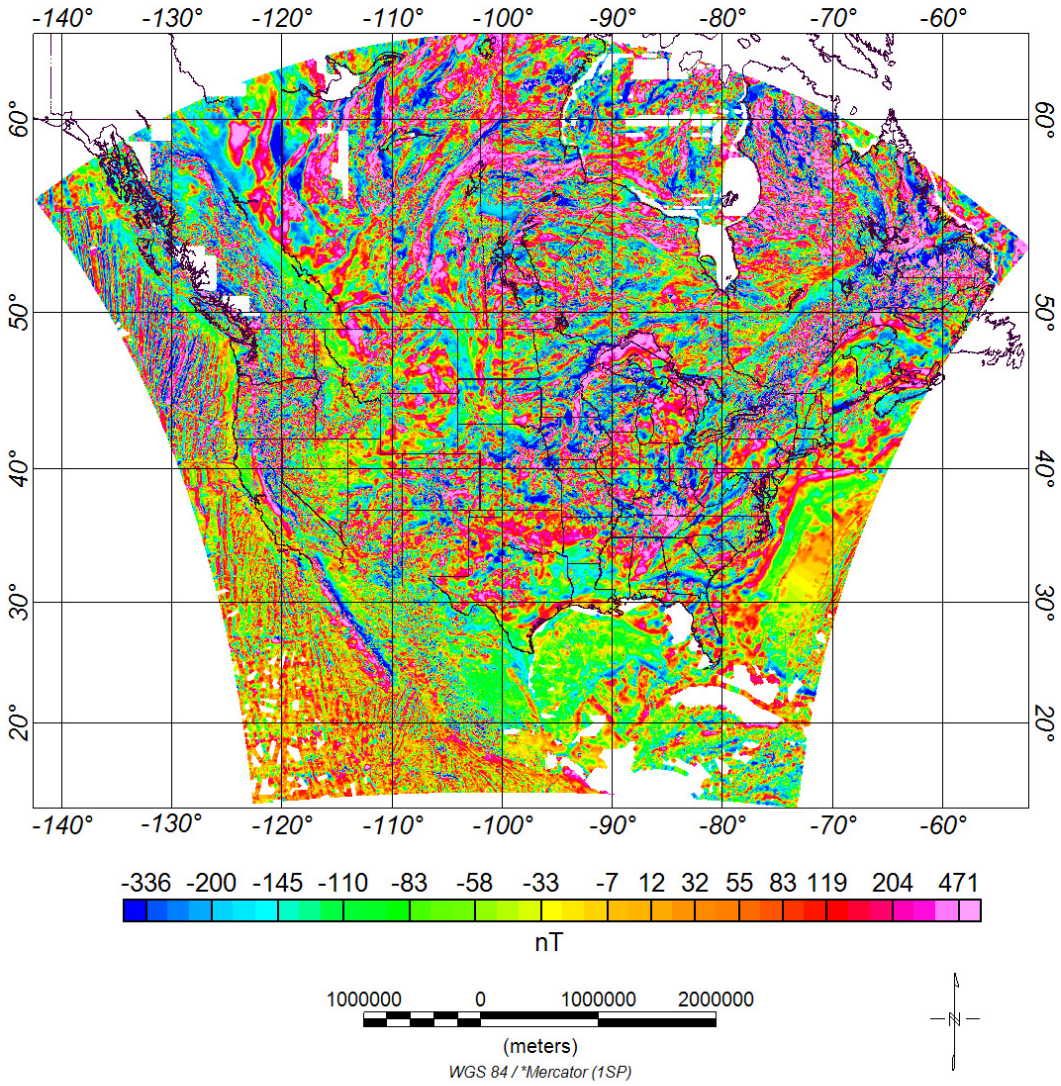

Figure 3.1 NURE_NAMAM2008 total intensity magnetic anomaly map.

NURE_NAMAM2008 Low-Pass 300 km

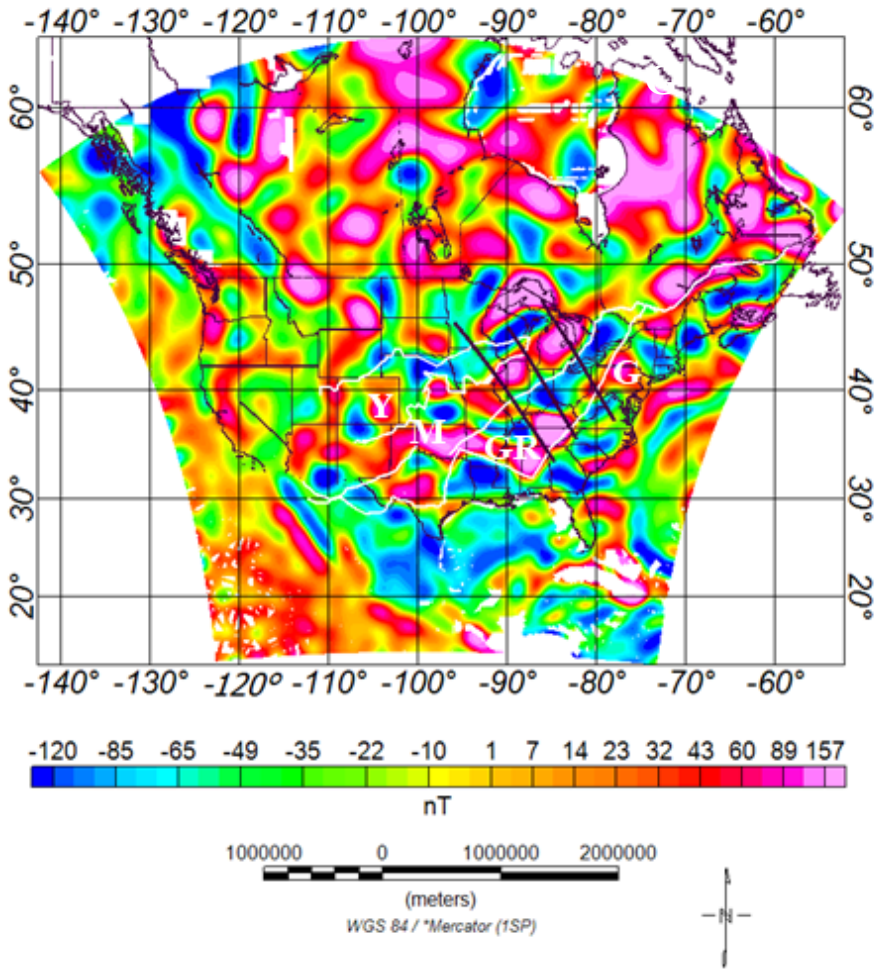

Figure 3.2 NURE_NAMAM2008 with 300 km low pass filter with profiles and province boundary lines as defined by Whitmeyer and Karlstrom (2007): M – Mazatzal, Y-Yavapai, GR – Granite Rhyolite, G – Grenville.

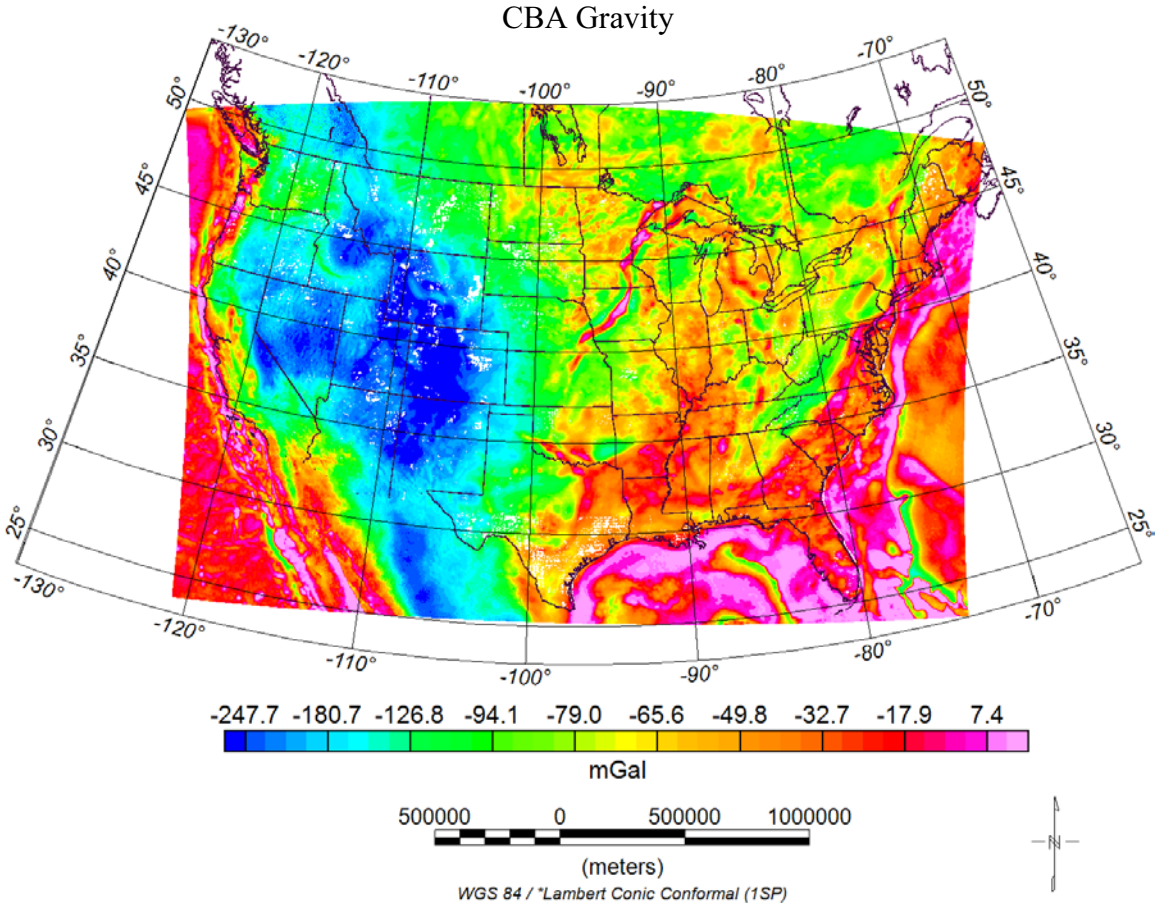

Figure 3.3 Complete Bouguer gravity anomaly map from PACES data combined with WGM2012 for the conterminous United States and the surrounding regions (H. L. Zhang, 2017, pers. comm.).

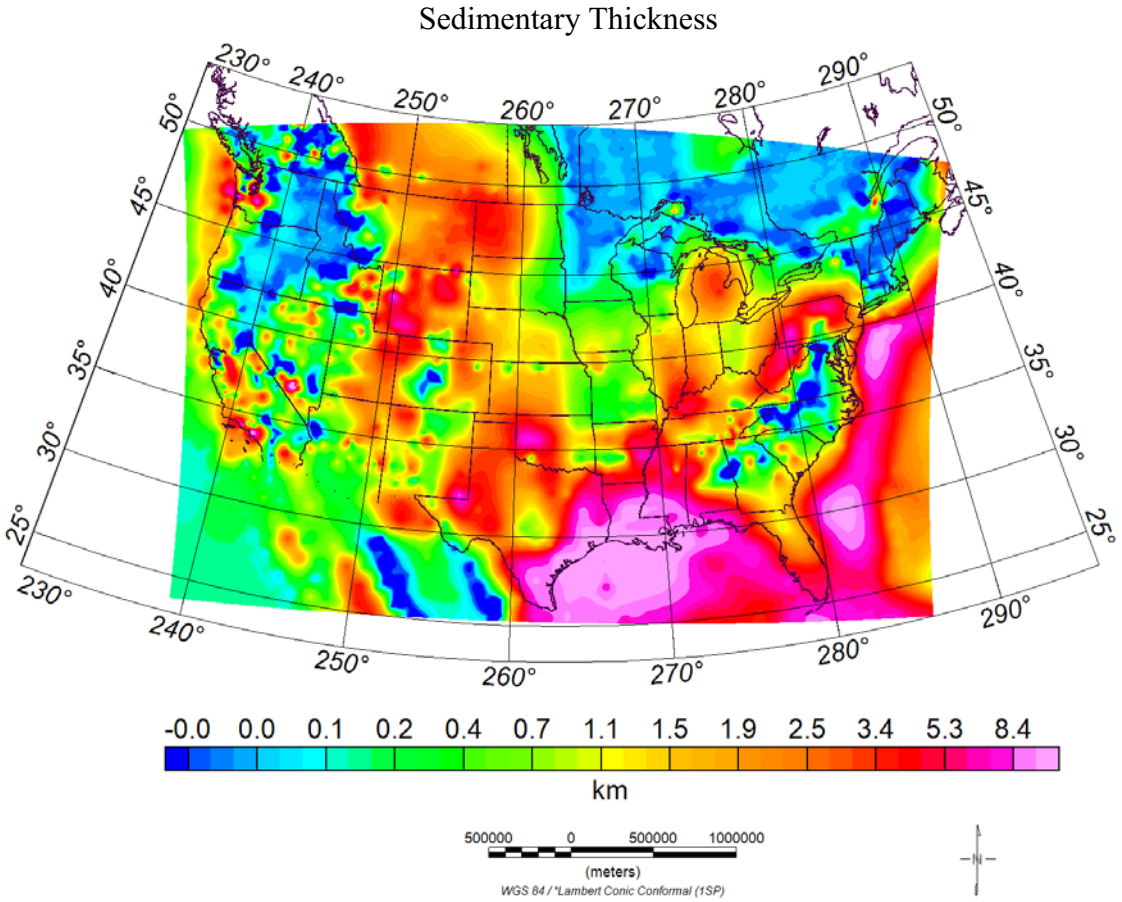

Figure 3.4 Sedimentary thickness (km) combined from different sources by Zhang (2017, pers. comm.).

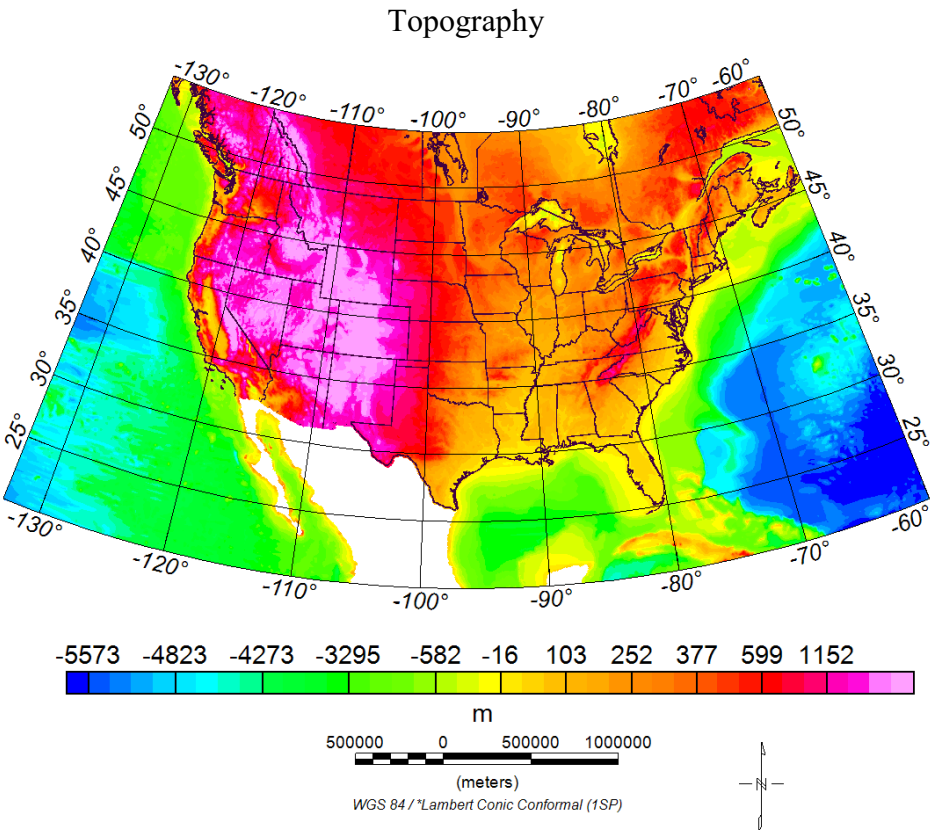

Figure 3.5 Topographic/bathymetry map of the conterminous United States and oceanic margins.

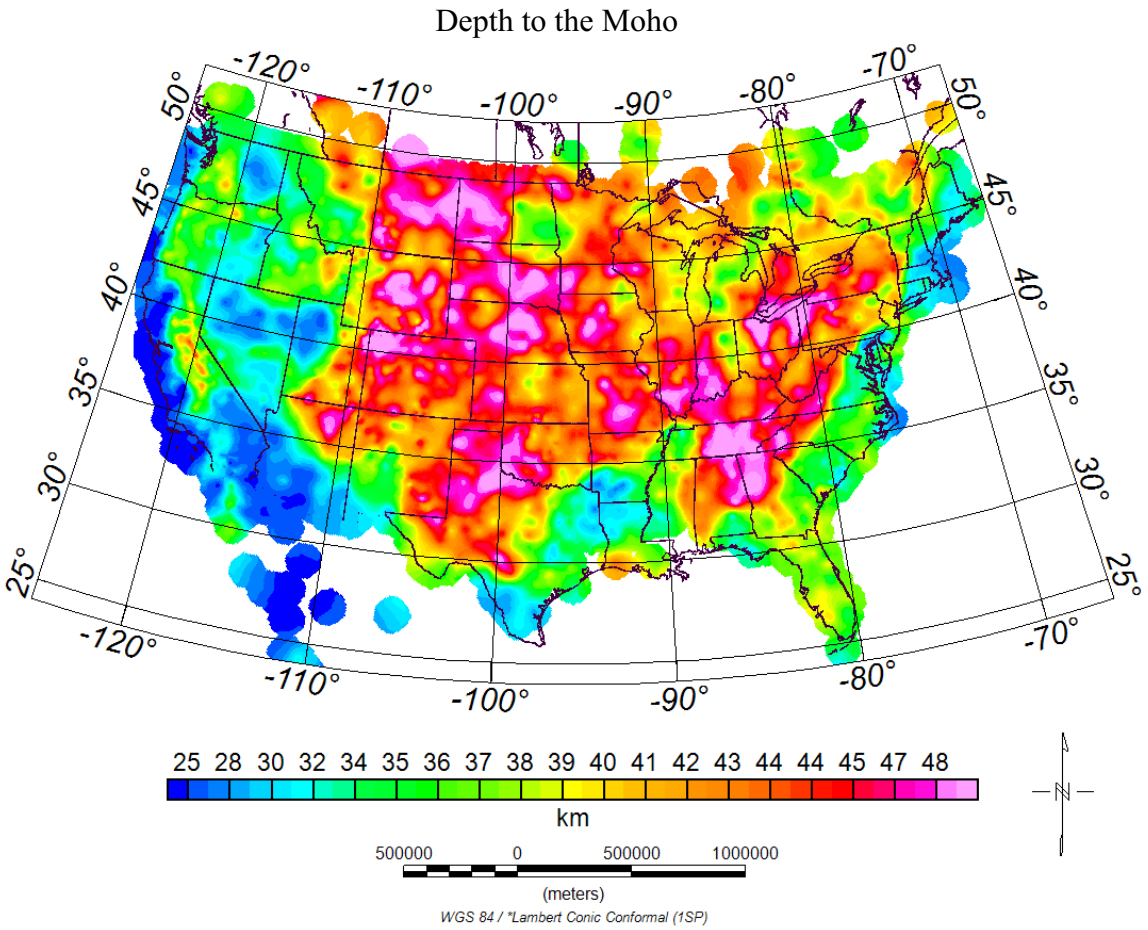

Figure 3.6 Crustal depth to the Moho (km).

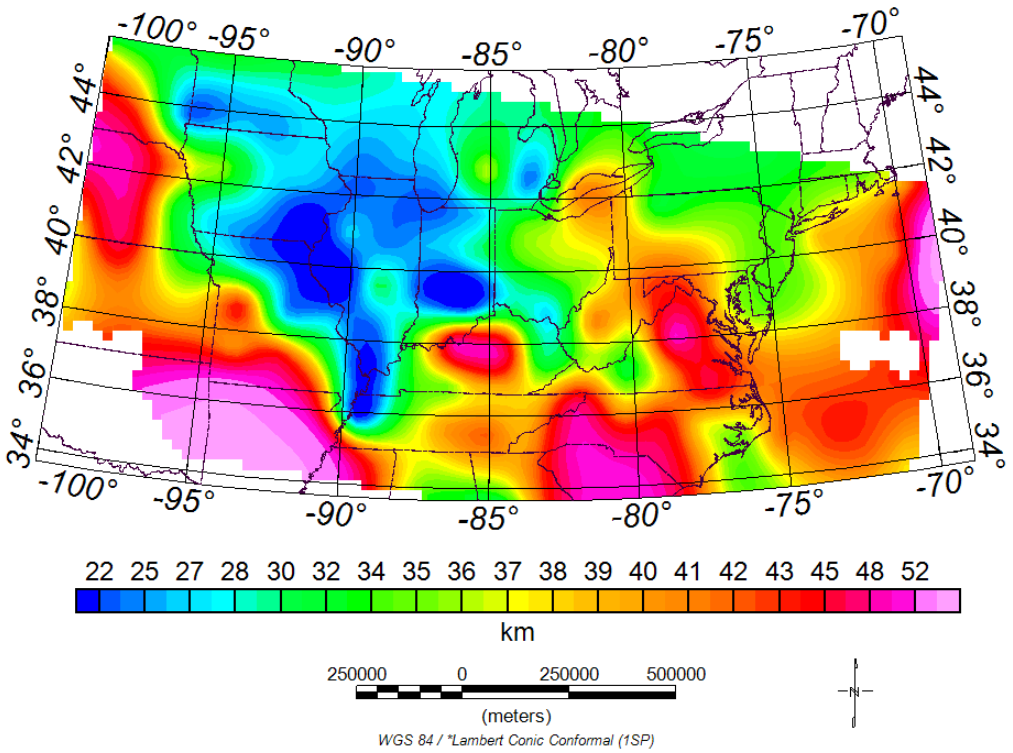

Figure 3.7 Spectrally-derived base of magnetization from the defractal method.

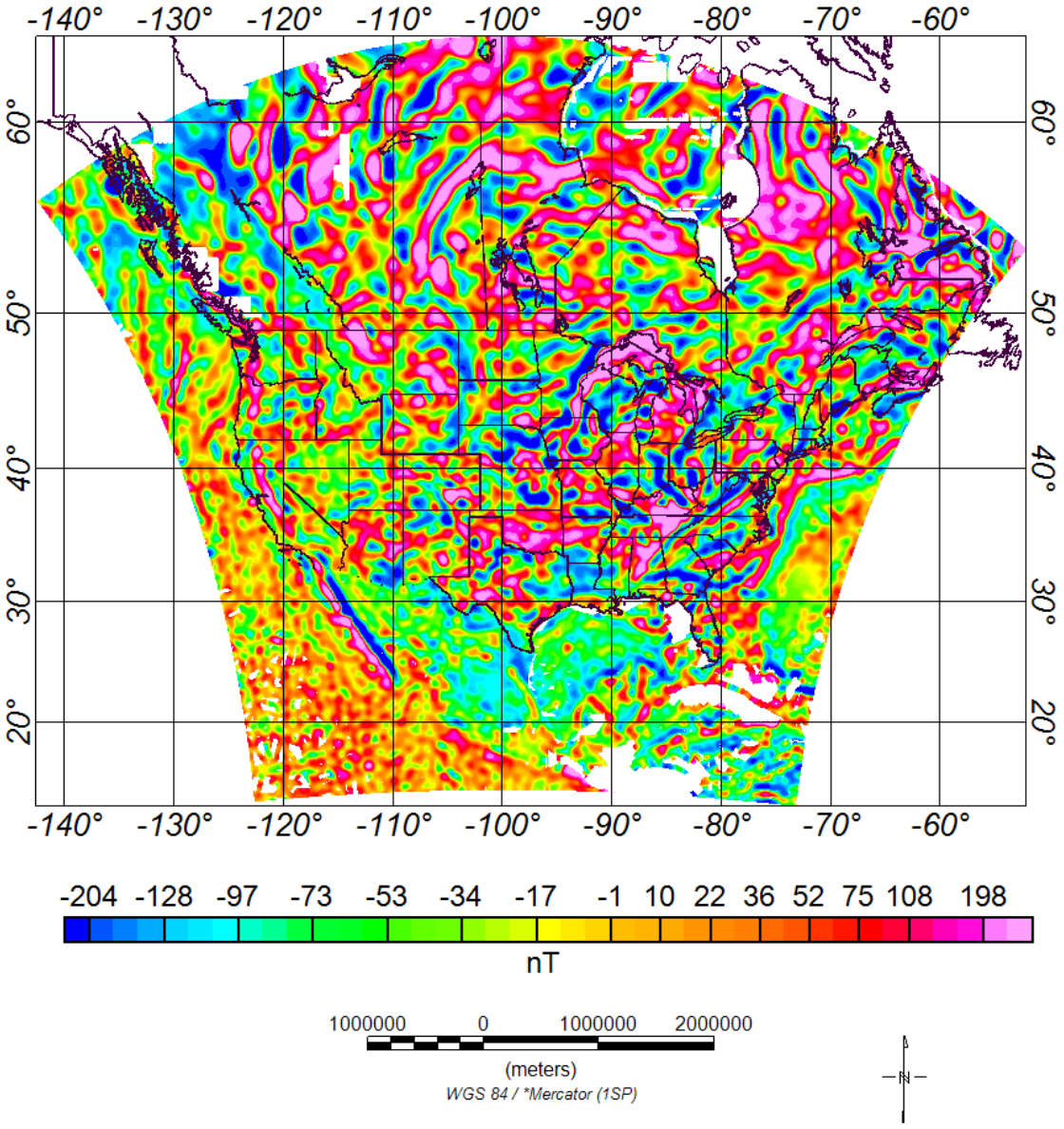

Figure 3.8 Low-pass filtered (100 km) NURE_NAMAM2008 magnetic anomaly map.

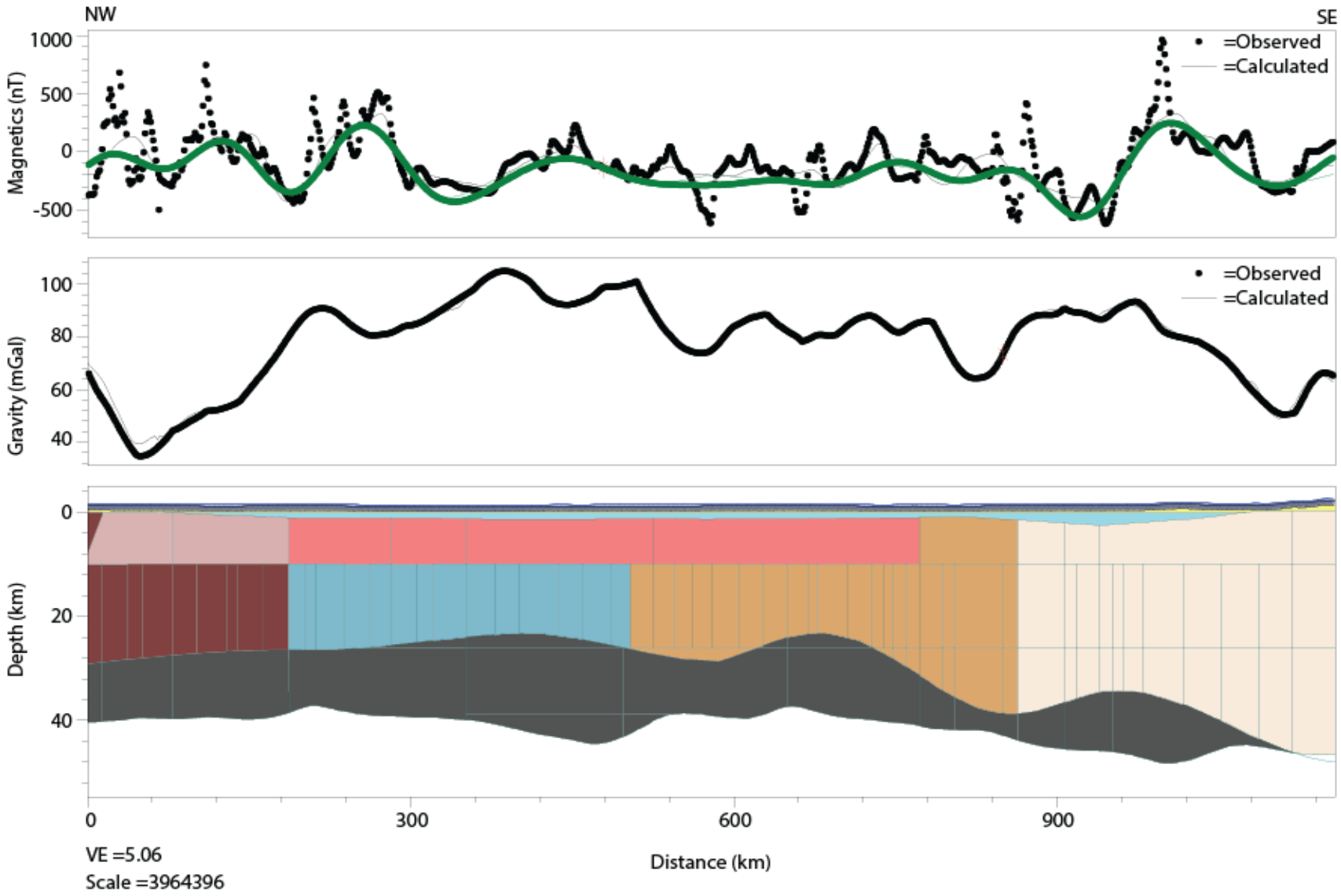
NW
SE
1000
500
0
-500
Magnetics (nT)
=Observed
=Calculated
100
80
60
40
Gravity (mGal)
=Observed
=Calculated
0
20
40
Depth (km)
0
300
600
900
Distance (km)
VE =5.06
Scale =3964396

Figure 3.9 Magnetic and gravity model demonstrating the fit of the large-scale crustal property variation to the 100 km low-pass filtered magnetic anomaly. Observed total intensity magnetic anomaly - filled black circles; 100 km low-pass filtered anomaly – thick green line; and 100 km filtered modeled anomaly (continuous black line). Gravity model and densities of different geologic units in all of the profiles are discussed in the text.

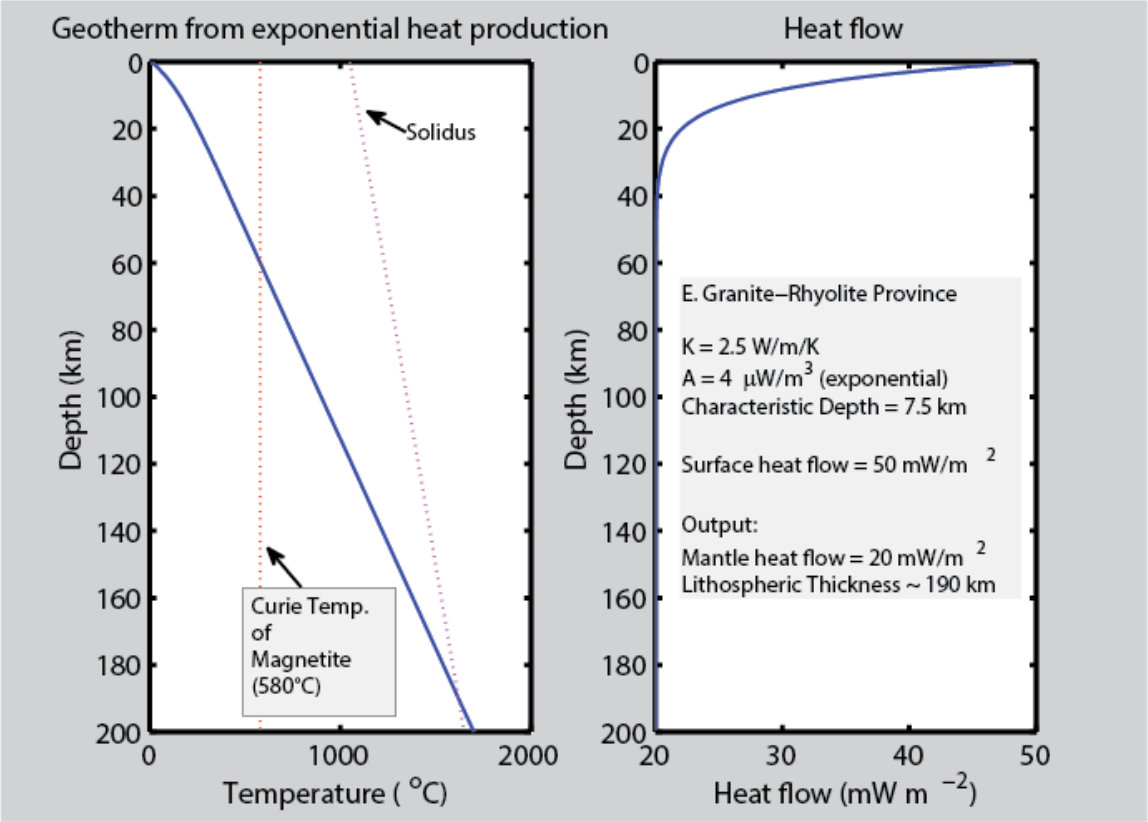

Figure 3.10. Geotherm and heat flow (Ravat, 2017, pers. comm.) used for constraining the depth extent of magnetized crust in the models with magnetized mantle.

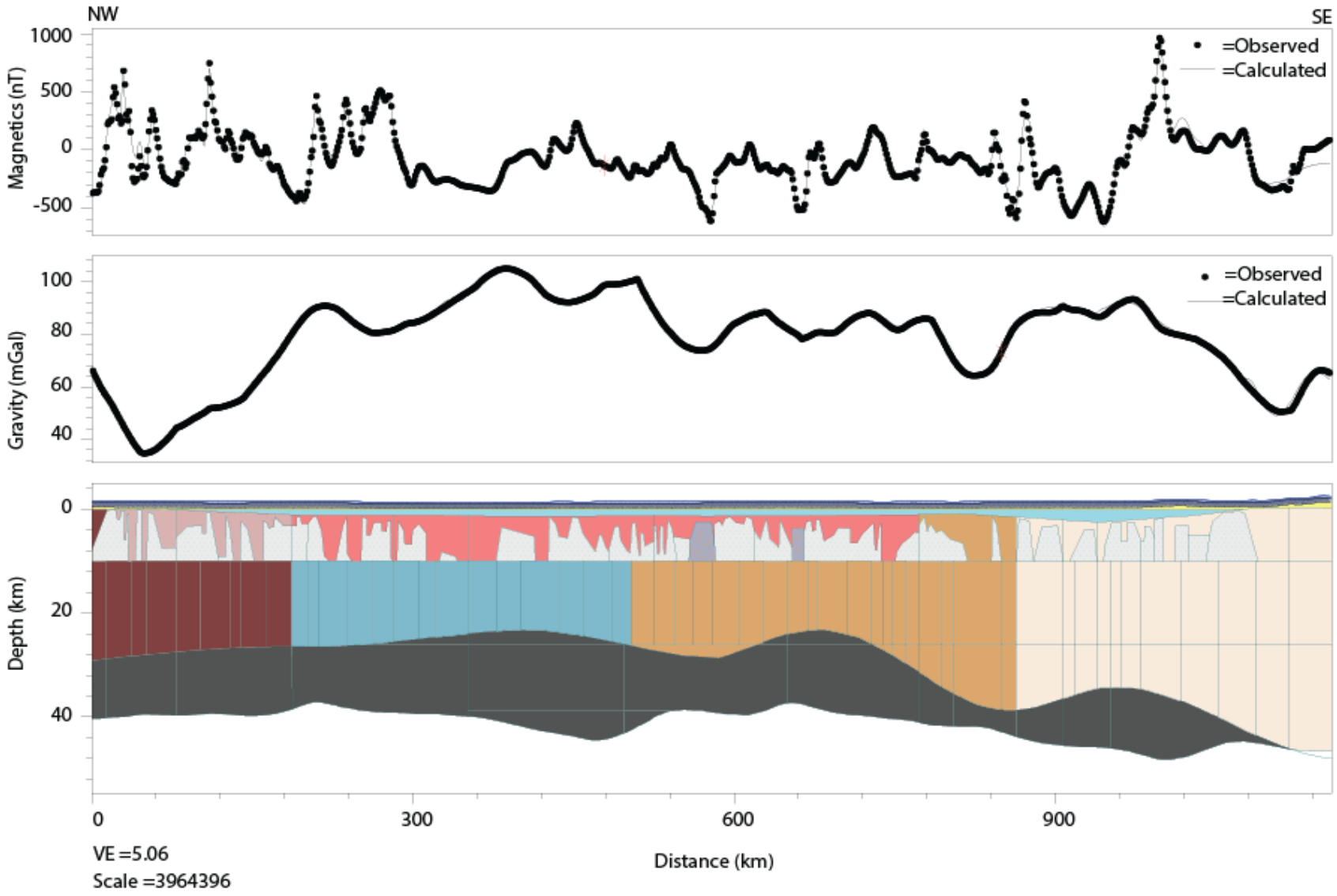
NW
SE
1000
500
0
-500
Magnetics (nT)
=Observed
=Calculated
100
80
60
40
Gravity (mGal)
=Observed
=Calculated
0
20
40
Depth (km)
0
300
600
900
Distance (km)
VE =5.06
Scale =3964396

Figure 3.11 Crustal magnetization model of ND_REFERENCE profile line.

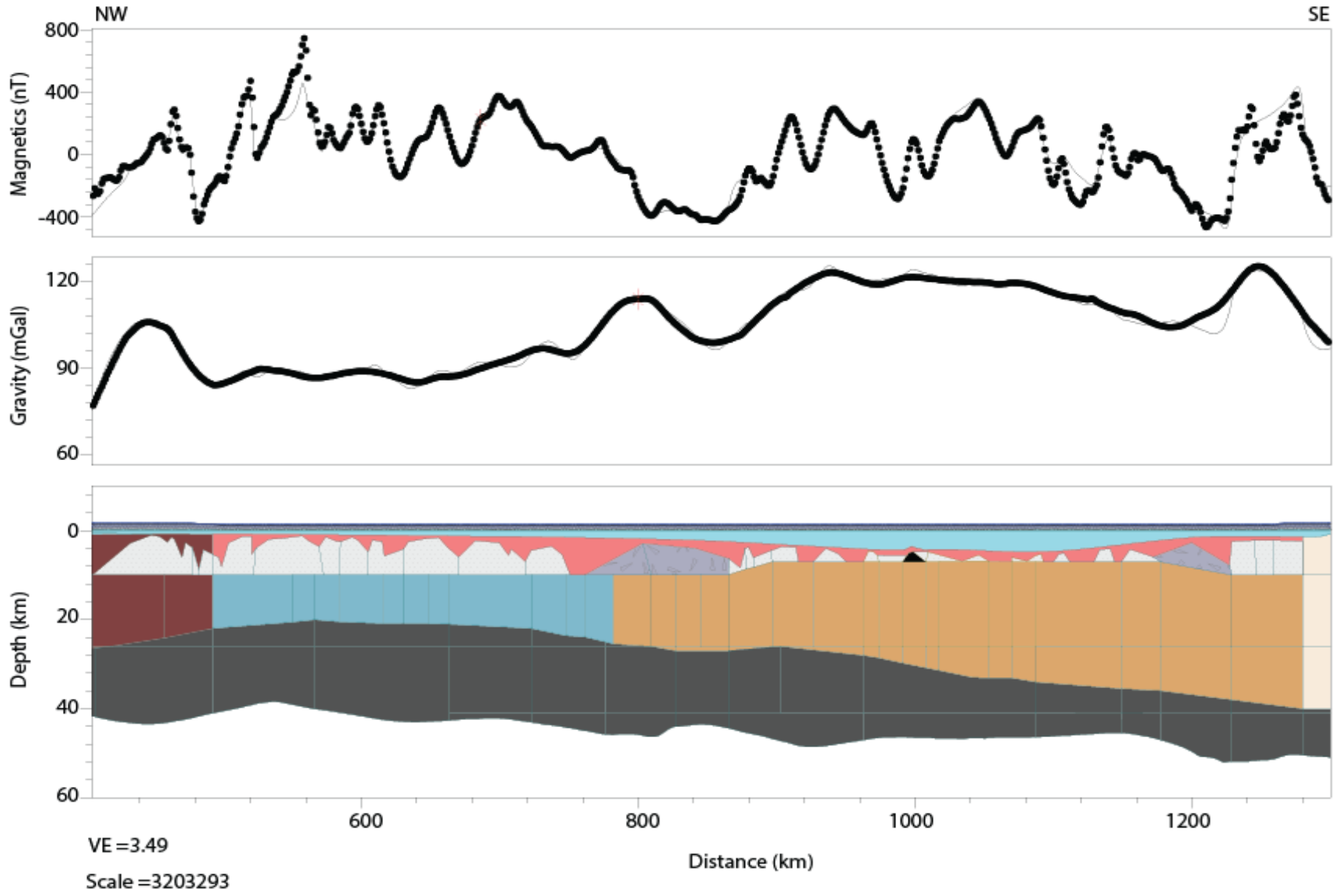
NW
SE
800
400
0
-400
Magnetics (nT)
120
90
60
Gravity (mGal)
0
20
40
60
Depth (km)
600
800
1000
1200
VE =3.49
Scale =3203293
Distance (km)

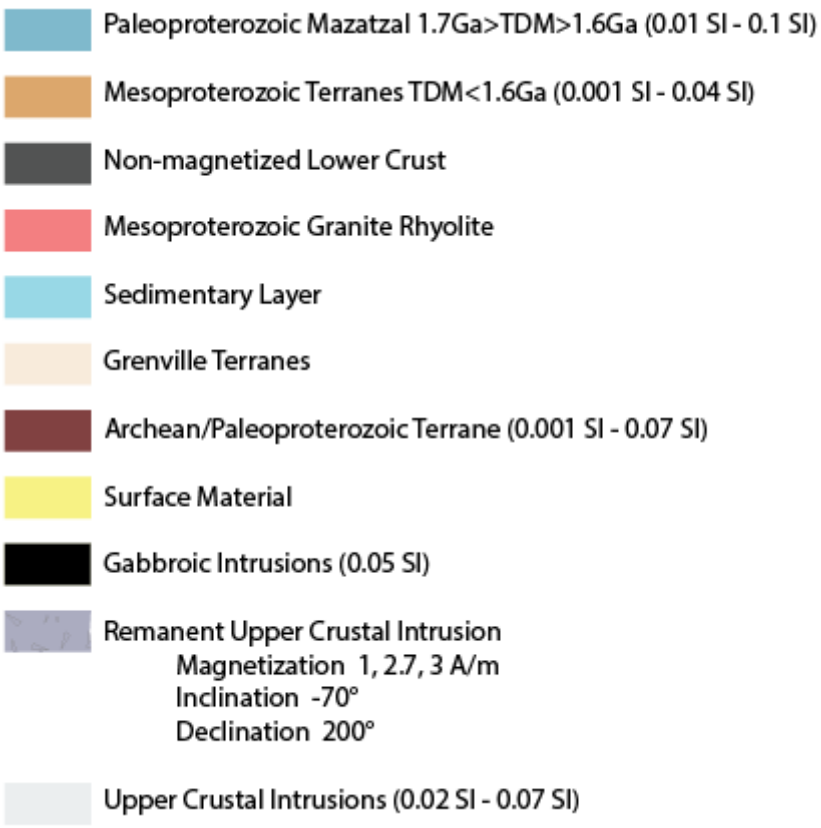

Figure 3.12 Crust-only magnetization of the ND_SW profile.

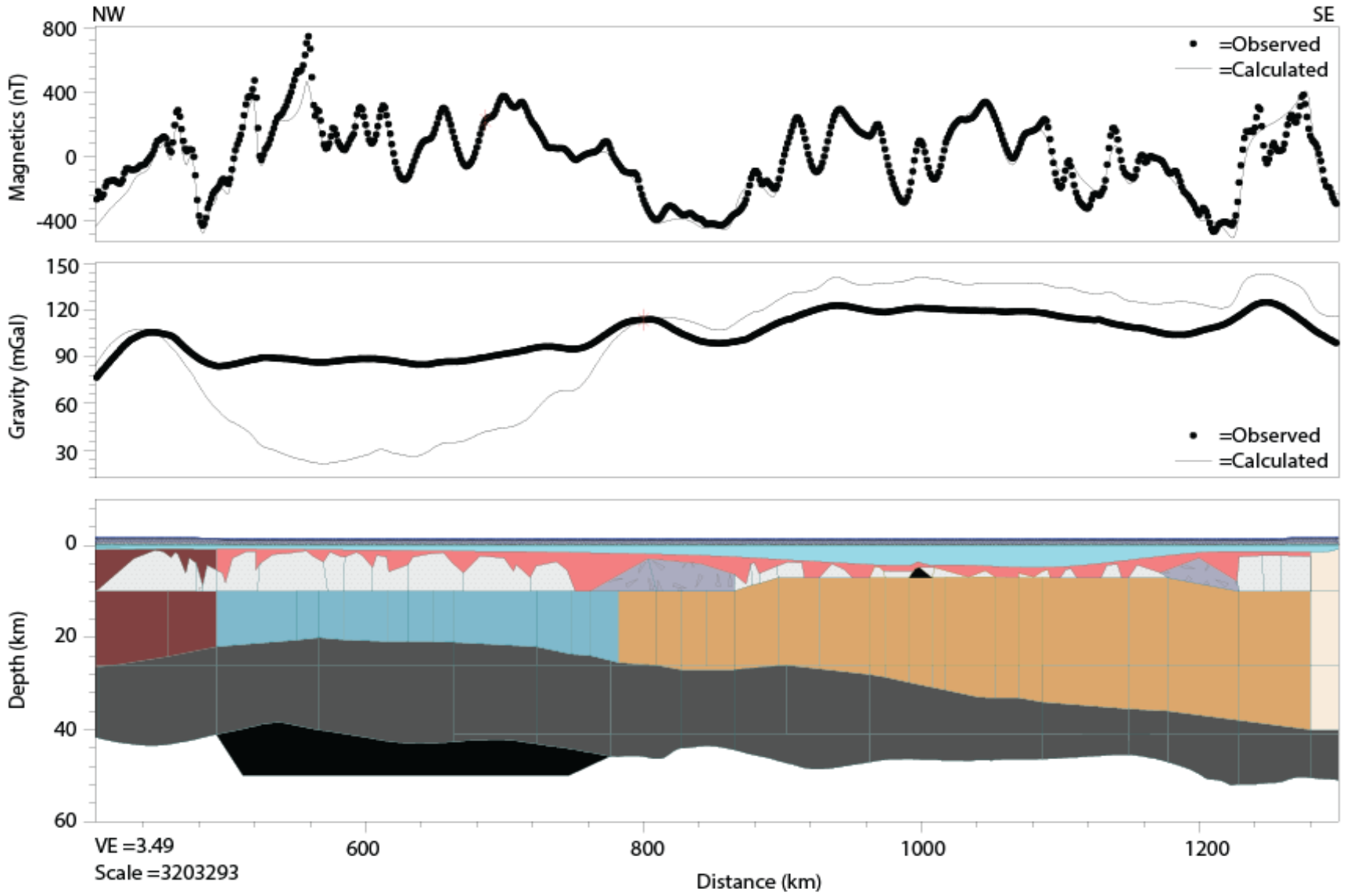
NW
SE
800
400
0
-400
Magnetics (nT)
=Observed
=Calculated
150
120
90
60
30
Gravity (mGal)
=Observed
=Calculated
0
20
40
60
Depth (km)
VE =3.49
Scale =3203293
600
800
1000
1200
Distance (km)

Figure 3.13 The model with underplated mafic mantle magnetization for the ND_SW profile. The gravity anomaly cannot be fit because of the addition of low density underplated material. Complex magnetic, non-magnetic magnetization-depth structure is required. This model is not considered plausible.

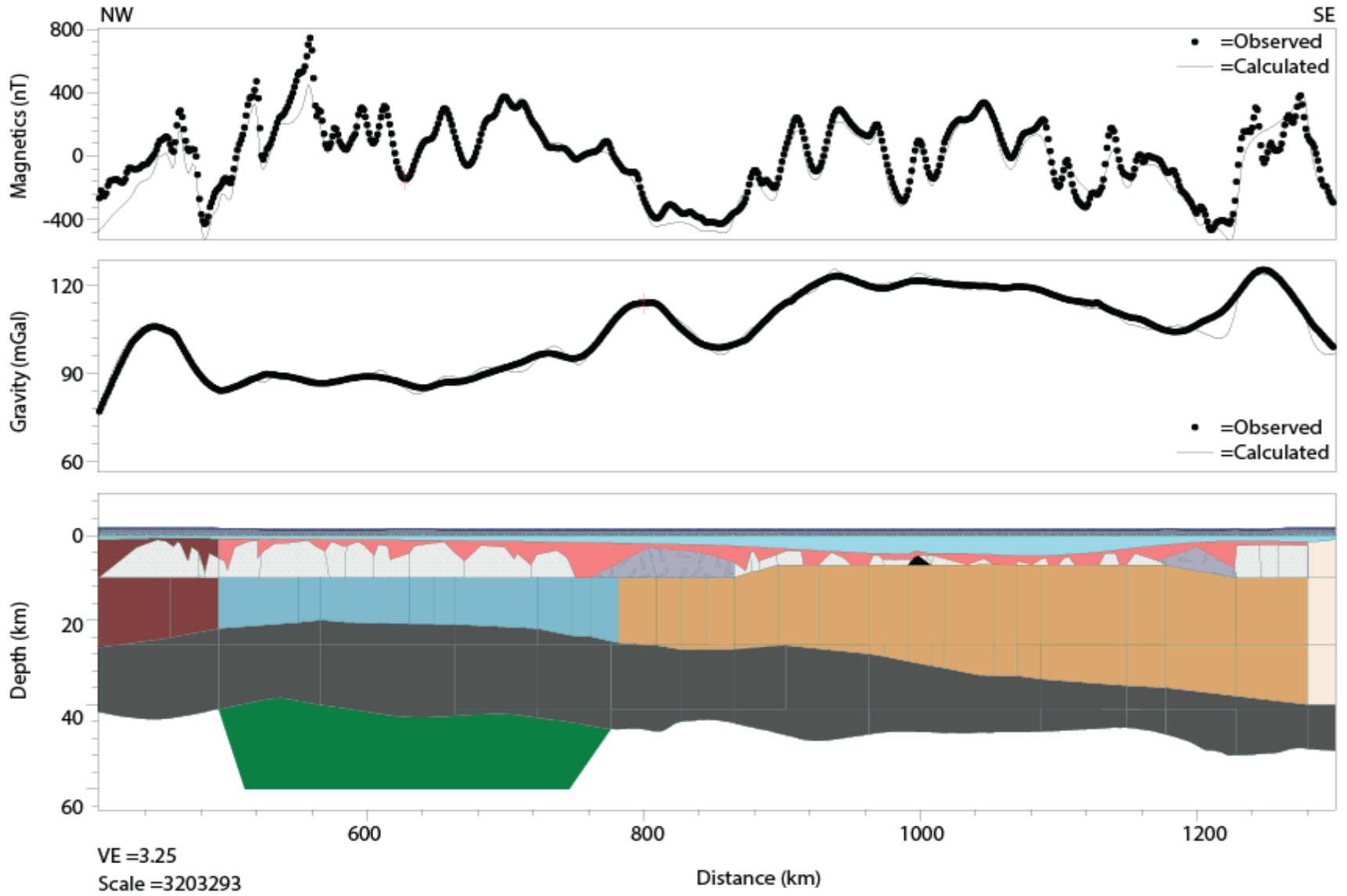
NW
SE
800
400
0
-400
Magnetics (nT)
=Observed
=Calculated
120
90
60
Gravity (mGal)
=Observed
=Calculated
0
20
40
60
Depth (km)
600
800
1000
1200
VE =3.25
Scale =3203293
Distance (km)

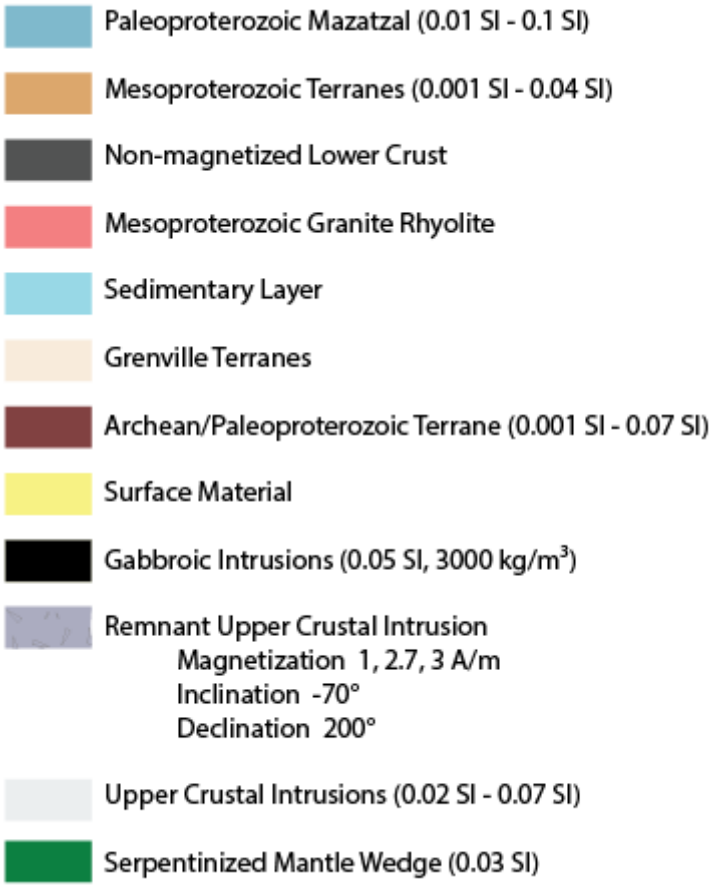

Figure 3.14 Once-serpentinized mantle source magnetization model for the ND_SW profile. Conceptual model involves a dispersed zone with magnetite within a polygonal region.

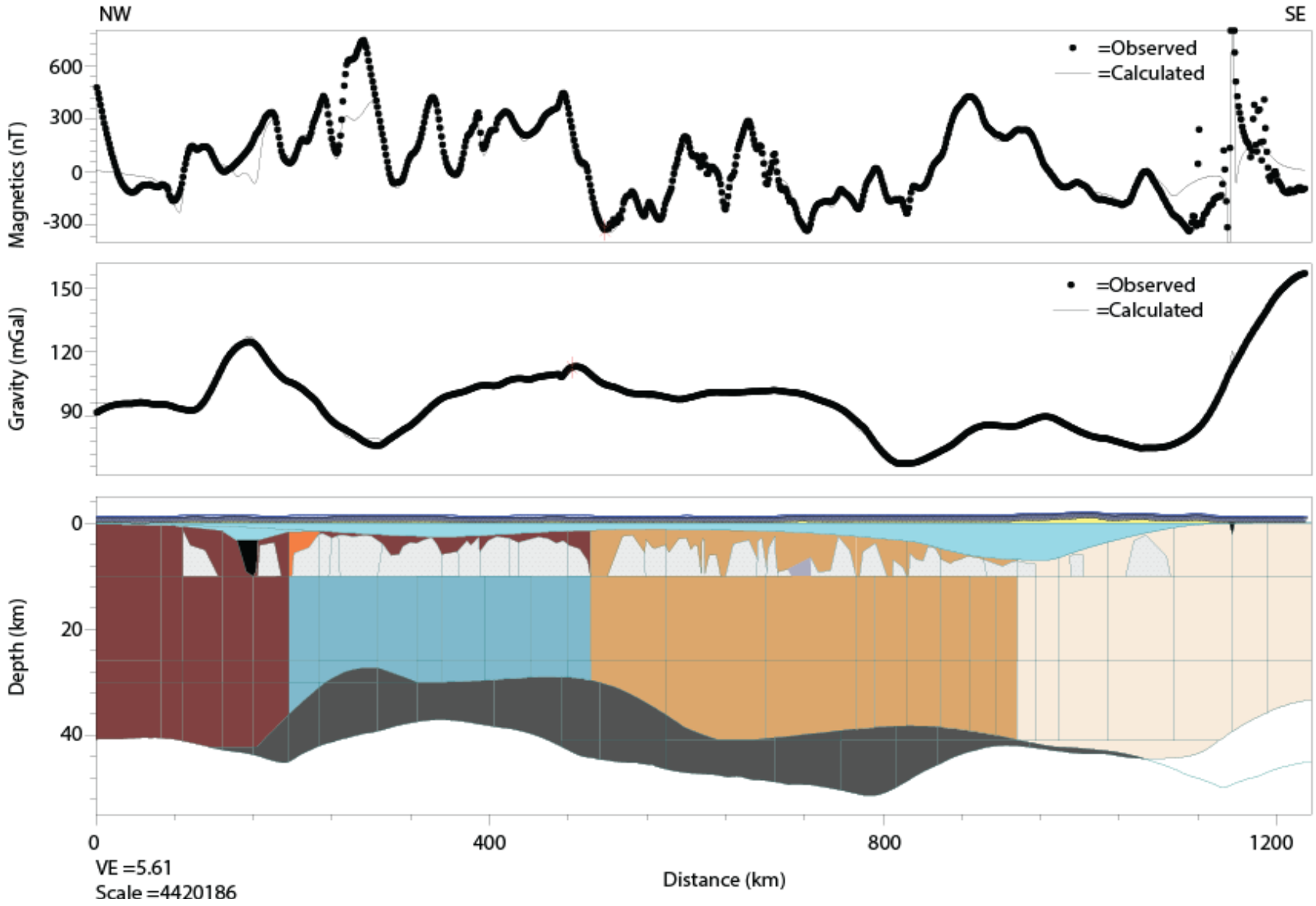
NW
SE
Magnetics (nT)
600
300
0
-300
=Observed
=Calculated
Gravity (mGal)
150
120
90
=Observed
=Calculated
Depth (km)
0
20
40
0
400
800
1200
VE =5.61
Scale =4420186
Distance (km)

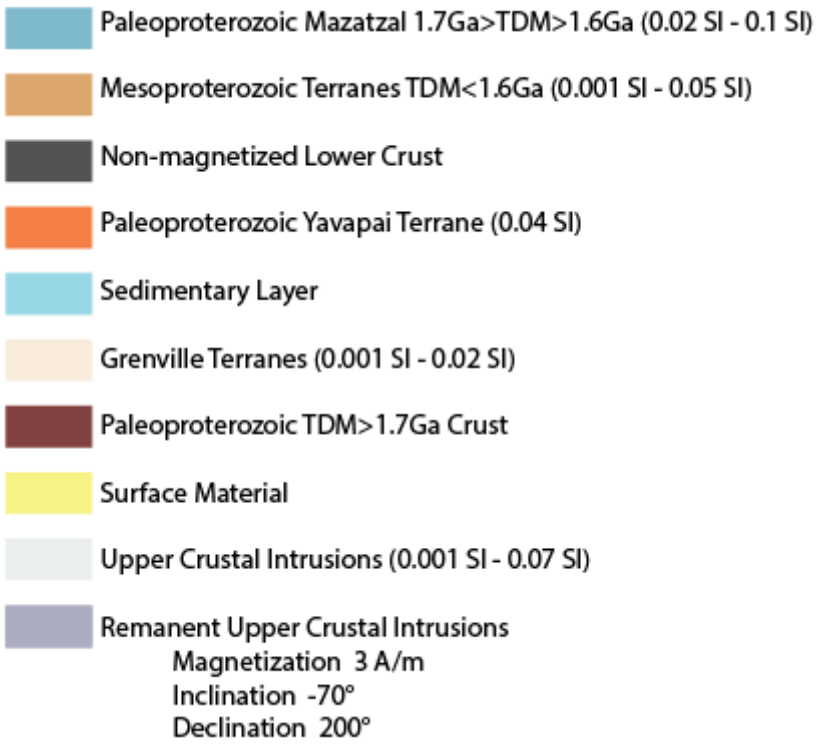

Figure 3.15 Crust-only magnetization model for the ND_NE profile.

Chapter 4 Discussion

A. Model ND_REFERENCE

Profile ND_REFERENCE (Figure 3.9; Figure 3.11) is the baseline profile because it lies in the quietest region sampling the magnetic anomalies over Paleoproterozoic and Mesoproterozoic terranes. The 100 km low-pass filtered magnetic anomaly was modeled first because it captures all the important crustal scale magnetic variations, many of which lie in the middle crust. The upper crust (shallower than 10 km) has no lateral susceptibility contrast (Figure 3.9). Middle crustal blocks range in susceptibility values from 0.001 to 0.09 SI and are consistent with diorites/tonalites (up to 0.07 SI) and gabbros (up to 0.1 SI) (Clark and Emerson, 1991; Clark, 1997; Clark, 1999), which are the two dominant rock types expected in this subduction/accretion setting. The highest susceptibility block in the middle crust forming the core of the Paleoproterozoic (T_{DM}) magnetic anomaly high has the susceptibility of 0.09 SI (blue block, 210 km to 240 km, Figure 3.9). Considering the increasingly mafic nature of the crust with increasing depth (Zandt and Ammon, 1995), this is reasonable. As the uppermost crystalline crust in the region is known to be more felsic (from basement samples in the eastern Granite-Rhyolite province), the models with unfiltered anomalies have a range limited to the highest susceptibility value for granites. There could be mafic upper crustal or near surface intrusions, such as the case of the Midcontinent Rift (MCR); however, with exceptions such as the MCR and a few special cases, the susceptibility values for granite were used.

Filtering of the calculated total intensity anomaly profile created by these blocks matches the 100 km low-pass filtered observed anomaly as well as its gradients and thus is consistent with the use of middle and deep crustal rocks as sources of strong long-wavelength magnetic anomalies (Figure 3.9). These middle crustal rocks form the high magnetization zone observed over the Paleoproterozoic (T_{DM}) Mazatzal province. The shorter wavelength features of the observed anomalies are then superimposed on this model with inclusion of upper crustal or near surface intrusions.

The largest deviation of calculated from the observed 100 km low-pass filtered anomaly is at 567 km along the profile (Figure 3.9). The calculated anomaly is about 90 nT higher than the observed. In the final unfiltered model, this region is modeled as a

block with remanent magnetization in the upper crust because even zero susceptibility was unable explain the anomalies in the region. In the total intensity magnetic anomaly, there are no clear features indicating the magnetization direction (induced or otherwise), and hence remanence opposite to the direction of the current field was used in the final model.

When comparing Proterozoic terranes, changes in both the depth to the Moho and the depth to base of magnetization are gradual in the Paleoproterozoic (T_{DM}) and older crust (e.g., Mesoproterozoic (T_{DM}) to the Paleoproterozoic (T_{DM}) provinces boundary at 504 km). Conversely, Grenville deformation and influence is identifiable in the Mesoproterozoic and Neoproterozoic terranes through the somewhat greater variation of the Moho and depth to base of magnetization relative to the older cratonic crust. The depth to base of magnetization deepens from roughly 26 km under the Paleoproterozoic (T_{DM}) magnetic anomaly to approximately 40 km under the westernmost Grenville province and the Paleozoic Appalachian Mountains (from 770 km along profile to the southeastern end). The older Paleoproterozoic terranes and Archean cratons have long since stabilized, whereas the Appalachian Mountains are from more recent Phanerozoic orogenies.

The gravity profile remains the same for both long-wavelength and unfiltered total intensity profiles. A prominent feature of the gravity profile is the significant low (34 mGal as opposed to approximately 80 mGal) in the northwestern region. Comparison to previous research and geologic maps identifies this low as part of the Wisconsin Wolf River Batholith (Allen, 1990; Allen and Hinze, 1992). Density and susceptibility values from these publications were compared to those used to model the profile. Thus, a low density upper crustal granitic batholith (less than 2800 kg/m^3) was independently inferred in both studies.

Figure 3.11 is the model that matches the unfiltered total intensity magnetic anomaly of ND_REFERENCE. The middle and lower crustal physical properties used in the 100 km low-pass filter model (Figure 3.9) and the modeling of unfiltered anomalies (Figure 3.11) are the same. Consistency of physical property values between the two models is important and provides constraints for mapping the remaining magnetization variations from short-wavelength anomaly features in the crystalline upper crust.

Susceptibility values for the middle crust for the unfiltered total intensity profile remain the same, ranging from 0.001 SI to 0.09 SI. These values all fall within the observed range of susceptibility for diorite (Clark and Emerson, 1991; Clark, 1997; Clark, 1999; Hunt et al., 1995) and are the lowest of all three profiles. The upper crustal intrusions were brought to the top of crystalline basement, not into the sedimentary layer above, for simplicity. Upper crustal intrusions on the ND_REFERENCE profile possess susceptibility values ranging from 0.01 SI to 0.07 SI and are consistent with susceptibilities of tonalities and diorites (Clark and Emerson, 1991; Clark, 1997; Clark, 1999; Hunt et al., 1995).

Superior/Yavapai (T_{DM}>1.7Ga) and Mazatzal (1.7Ga>T_{DM}>1.6Ga) Paleoproterozoic provinces (Figure 3.11, from 0 km to 500 km on the profile) have susceptibility values from 0.001 SI to 0.09 SI. The Mesoproterozoic (T_{DM}) and Neoproterozoic provinces extend from 500 km to the end of profile. Values are generally low, from 0.001 SI to 0.05 SI for the middle crust and 0.001 SI to 0.06 SI until the Grenville front at 860 km. The boundary was determined from geochemically-defined province maps (Whitmeyer and Karlstrom, 2007; Bickford et al., 2015). In the Grenville terranes, however, susceptibilities increase ranging from 0.001 SI to 0.07 SI in the middle crust with upper crustal intrusions from 0.03 SI to 0.07 SI. Certain middle crustal blocks have very low susceptibilities (0.001 SI to 0.01 SI). They occur at 500 km and 860 km and separate the Paleoproterozoic (T_{DM}) Mazatzal from Mesoproterozoic (T_{DM}) within the Granite-Rhyolite province and the Mesoproterozoic (T_{DM}) from younger Grenville, respectively. These blocks of low susceptibility could possibly be related to high pressure deformation at the suture zones between the Paleoproterozoic (T_{DM}) and Mesoproterozoic (T_{DM}) age terranes. Modeled susceptibility averages of middle crustal units were calculated for the Paleoproterozoic Yavapai (T_{DM}), Paleoproterozoic Mazatzal (T_{DM}), Mesoproterozoic (T_{DM}), and Grenville regions. Interestingly, the Yavapai had the highest average susceptibility with 0.07 SI despite its low-pass filtered low anomaly region (Figure 3.2) and high amplitude high variability unfiltered anomalies (Figure 3.11); the reason for these high middle crustal susceptibilities is the low upper crustal susceptibilities of the large Wolf River Batholith which has significant volume. The middle crustal susceptibility averages are 0.04 SI for Paleoproterozoic Mazatzal, 0.01 SI

for the Mesoproterozoic terranes, and 0.02 SI for the Grenville (Table 4.1). As this profile lies in the quietest region sampled along the Nd line, it establishes the minimum average susceptibility for the Paleoproterozoic Mazatzal province in this region. Because the other two profiles have higher average susceptibility values in the middle crust within their Paleoproterozoic (T_{DM}) Mazatzal domain, they could represent greater magmatic activity or intervening high susceptibility terranes during the accretion of a series of island arcs onto the southeastern margin of Laurentia (Whitmeyer and Karlstrom, 2007).

B. Model ND_SW

ND_SW is the original profile modeled and different high magnetization scenarios were tested on it. The crust-only magnetization model (Figure 3.12) illustrates characteristics similar to those seen in ND_REFERENCE. It crosses different geologic regions over its 1200 km length, one of these being the Illinois Basin with depths at its greatest extent reaching over 5 km. Surprisingly, the gravity and magnetic anomalies over the basin spanning from 865 km to 1190 km are higher than the lows on either side. This is an unexpected result because of the depth of the Illinois Basin. The negative density contrast caused by sedimentary material compared to the crystalline basement surrounding it should lead to a gravity low unless compensated at the Moho. The magnetic and gravity anomaly lows on either side of this Mesoproterozoic high potentially represent suture zones between the Laurentian craton and accreting arc material (Thomas et al., 1987). Subduction is known to have occurred along this border of Laurentia throughout the Proterozoic (Whitmeyer and Karlstrom, 2007). Early collisional events produced the Trans-Hudson and Yavapai orogenies during the early Paleoproterozoic and culminated in the amalgamation of Rodinia at the beginning of the Neoproterozoic (Whitmeyer and Karlstrom, 2007).

In modeling gravity anomaly high over the basin, the Moho density contrast and the observed Moho upwarp was not sufficient and the top of the middle crust was elevated by approximately 3 km. ND_SW is the only profile that illustrates the elevated middle crust to compensate for the largest sampled sedimentary basin of all three profiles. However, middle crust with higher densities could also explain the gravity high. There is a small triangular feature at 1000 km (3 km depth) in the bottom of the basin that has

corresponding gravity and magnetic highs. The depth of the crystalline basement in the Illinois basin (Figure 3.12) was taken from the detailed 3D compilation of Ellett and Naylor (2016); however, the small upwarp of the crystalline basement is insufficient to reproduce the magnetic anomaly.

Magnetic susceptibility values are significantly higher under the Paleoproterozoic region than the Mesoproterozoic region. This is necessary due to the boundary constraints imposed by the depth to the base of magnetization and the sedimentary layer above. In all three profiles, the magnetizable part of Paleoproterozoic crust is much thinner than in the Mesoproterozoic. Middle crustal average susceptibility for ND_SW is highest in the Paleoproterozoic (T_{DM}) Mazatzal (0.06 SI), the older Paleoproterozoic Yavapai/Superior average susceptibility is 0.03 SI, it is 0.01 SI for the Mesoproterozoic (T_{DM}) Eastern Granite-Rhyolite, and finally the Grenville has the smallest average susceptibility (0.008 SI) (Table 4.1).

Deep sedimentary basins appear to pose several modeling challenges. In the Paleoproterozoic upper crust, the susceptibility of the upper crustal intrusions are at their maximum value for granites as well as those for the dioritic middle crustal blocks below. From 534 km to 567 km of Figure 3.13, the calculated magnetic anomaly does not match the full amplitude of the observed anomaly despite the susceptibility being the maximum value for diorite (0.1 SI). If the intrusions were modeled into the sedimentary layer, the calculated anomaly and its gradient would match the observed. As this study used the thickness of the sedimentary layer as a constraint for the top of the magnetic layer, models where the intrusions penetrate the sedimentary layer were not evaluated; however, the possibility exists as intrusions are present throughout the mid-continent, products of Granite-Rhyolite province related to younger Neoproterozoic and Paleozoic magmatism (Whitmeyer and Karlstrom, 2007). Upper crustal intrusions are indeed observed in the midcontinent region, in particular, the Green Island Plutonic Belt in southwestern Iowa that is of Mesoproterozoic crystallization age. Sm-Nd analysis of samples from these rocks indicates intrusion through older continental crustal of Paleoproterozoic (Mazatzal) age (Holm, 2007; Van Schmus et al., 1993, Van Schmus et al., 1996). Moreover, near surface dike complexes have been observed in Illinois and

Indiana including intrusives in Hicks Dome and Omaha Dome (Hildenbrand and Ravat, 1997).

B1. ND_SW Underplated Mafic Material Source

The original crust-only magnetization ND_SW profile was modified to include a mantle source of underplated basaltic material (Figure 3.13). Mafic underplating is a known process in areas of subduction where the mantle melts due to interaction with water from the dehydrating slab and forms a pool of mafic material (Fyfe, 1991; Thybo and Artemieva, 2013). The process has been inferred from scattered returned seismic signal thought to be caused by the underplated material (Thybo and Artemieva, 2013). Melting of the mantle can produce gabbroic material responsible for the production of magnetite in the hydrating environment. If the source of magnetization on the Paleoproterozoic side of the T_{DM} line is related to pooling of gabbroic material at the base of the crust, several features that result from this less dense highly magnetic material are expected. This basal crustal material could have a probable maximum susceptibility of 0.04 SI (Clark and Emerson, 1991; Clark, 1997; Clark, 1999). Having reached the maximum susceptibility value for diorite in the middle crust (0.1 SI, Clark and Emerson, 1991; Clark, 1997; Clark, 1999) requires about 5 km thick mafic underplating with the susceptibility of 0.03 SI in order to match the magnetics. While the result from emplacing a small thickness mafic layer (less than 5 km thick, and this is within the error range of seismic receiver function estimates of the Moho) produces the expected stronger magnetic anomaly in the region directly above, it also leads to approximately 50 mGal calculated gravity anomaly low than the crust-only magnetization model. This is because the mafic underplated mafic material would have density similar to the basal lower crust (3000 kg/m^3 in comparison to the mantle 3300 kg/m^3 in Figure 3.13). The calculated magnetics, though now boosted by the underplated crustal source, still do not match the full amplitude of the observed.

B2. ND_SW Once-Serpentinized Mantle Wedge

The second mantle source scenario is a zone of once-serpentinized mantle material created through metasomatization of the forearc mantle wedge by a subducting oceanic slab (Figure 3.14). While this process is presently known to occur in collisional settings through identification of a magnetic anomaly high and a corresponding gravity

anomaly low due to the low density but highly magnetic serpentinized peridotite in the forearc (Blakely, 2005; Bostock et al., 2002; Hyndman and Peacock, 2003), the largest obstacle to this scenario is age. It is possible that processes occurring during the initial formation of the Mazatzal led to the resulting properties expressed as this magnetic high today. A serpentinized mantle wedge 1.6 billion years ago could have created high susceptibility material at the base of the crust. After the end of subduction, hydrating conditions would cease and temperatures within the forearc gradually increase causing serpentinite to revert back to peridotite. However, the magnetite formed during the serpentinization will remain magnetite and would mix with the surrounding mantle over 1.5 Ga. For simplicity's sake, this dispersed zone of once-serpentinized uppermost mantle magnetite was modeled as a polygon at the base of the crust with a susceptibility of 0.03 SI (middle of the range of serpentinized peridotite, Clark and Emerson, 1991; Clark, 1997; Clark, 1999). The resulting calculated magnetic anomaly matches the observed closer than the mafic underplating model, but not as well as the crust-only model. For example, the magnetic gradient at 490 km becomes steeper and does not match as well as the crust-only model. However, it does raise the base levels to where a mantle source of once-serpentinized material could help match the observed magnetic anomaly profile. While an intriguing scenario, the drawback of age and the knowledge of current geometric configuration are large factors.

The magnetite created from the process of serpentinization would remain and continue to be magnetic unless mantle temperatures at the base of the crust surpass the Curie temperature of magnetite (580º C). According to the base of magnetization determinations with large spectral windows (up to 1000 km) which average information over very large region and cannot precisely identify locations of the base of magnetizations, magnetite could exist in a ferromagnetic state up to 60 km depth, well below the Moho on all three profiles (D. Ravat, 2017, pers. comm.). Modeling of heat flow in the region, taking into account high radiogenic heat production of granites in Granite-Rhyolite provinces also yields a depth of about 60 km for reaching 580°C (see the geotherm in Figure 3.10). Lacking surface or drillhole samples in the mid-continent that bear clues to this process or lacking other geophysical evidence from the mantle depths makes this scenario difficult to corroborate and thus is not considered further.

C. Model ND_NE

ND_NE is the northernmost of the three models, and it is affected by ? the most influence from near-surface geological sources outside of the model (Figure 3.15). This profile catches the Midcontinent Rift at its northwesternmost extent, and as such, the magnetic anomalies in that region are influenced by the strong effects of near-surface gabbro and basalt. The trend of the Midcontinent Rift is also parallel to the profile whereas the model is 2D perpendicular to the profile. Susceptibilities in the Paleoproterozoic (T_{DM}) anomaly region as well as the region encompassing the older Superior Craton are very high, ranging from 0.03 SI to 0.1 SI with more than 50 percent of the sources modeled in the middle crust above 0.05 SI. This is likely to compensate for the shallow Moho and the depth to the base of magnetization in the region. Because of the uplift in the Moho (195 km to 495 km along the profile), there is less room for middle crustal blocks to hold magnetization. Consequently, the middle crustal susceptibilities of the Paleoproterozoic blocks must be very high in order to honor this constraint.

The upper crustal intrusions, like both other profiles, are only modeled to the top of crystalline basement. Similar to ND_SW, the calculated magnetic anomaly profile for ND_NE does not match the observed for some of the anomaly features. While the intrusions residing only within crystalline basement are not enough to produce matching anomalies, if they could penetrate into the sedimentary layer, both profiles would match and provide a better fit. Maximum observed susceptibility values for diorite (0.1 SI, Clark and Emerson, 1991; Clark, 1997; Clark, 1999) are used in middle crust under the zone of high magnetization where the observed/calculated mismatch occurs. The calculated magnetic anomaly profile could be made to match; however it would require large values beyond susceptibility values observed for diorite. Borehole samples of the crystalline basement rocks or a high resolution seismic reflection profile that captures the basement at that location would be required in order to ground truth the validity of this inference.

ND_NE follows the same pattern as the other two profiles in regards to the susceptibility pattern of the mid crustal blocks. The T_{DM}>1.7Ga Paleoproterozoic terrane shows the second highest susceptibility (Table 4.1) with the average of 0.06 SI, the

1.7Ga>T_{DM}>1.55Ga Paleoproterozoic blocks have the average of 0.07 SI (the highest for this profile), the average of 0.02 SI for T_{DM} <1.55Ga Mesoproterozoic terrane, and 0.009 SI for the Grenville. A small low susceptibility region between 500 and 580 km is 0.001 SI between the Paleoproterozoic (T_{DM}) Mazatzal and the Mesoproterozoic (T_{DM}) terranes could potentially represent a suture zone of younger arc material onto the margin of the old craton and may represent zone of high pressure deformation. Also like the two other profiles, there is a lack of correlation between the gravity and magnetic anomalies other than in select regions such as the MCR. Gravity anomaly data does not provide distinctive trends like the magnetics does. The occasional alignment of a gravity and magnetic anomaly high likely indicate the presence of a pluton (Figure 3.13, 990km to 1008 km, 7km depth).

On model ND_NE, the deep sedimentary basin of the Rome Trough (Figure 3.15, 815 km to 1085 km, 7 km deep) shows gravity highs in the region expected to have a gravity low. The lower density of the sediments combined with the uplifted isostatically-compensated Moho required higher middle and lower crustal values in order for the calculated gravity anomaly to match the observed gravity anomaly. When the amount of expected mantle upwarp to isostatically compensate for the low density basin was simplistically calculated using

$$b = \frac{(\rho_c - \rho_s)}{(\rho_m - \rho_c)} h \quad (9)$$

(where b is the expected mantle upwarp, ρ_c is the density of the crust – 2820 kg/m^3, ρ_s is the density of the sediments – 2600 kg/m^3, ρ_m is the density of the mantle –3300 kg/m^3 , and h is the depth of the sedimentary basin – 7km)(963 km, 7 km depth, Figure 3.15) (Watts, 2001); the Moho is overcompensating the depth of sediments by approximately 5 km. This overcompensation explains the local gravity anomaly high in the regional gravity anomaly low spanning the Rome Trough region. This is a simplistic way to determine the isostatic balance of the region as the observed data do not represent perfect block models.

The isostatic balance was also examined using the weighted average density of a crustal column in the middle of basin and on the side in stabilized crust. Average densities for ND_NE were calculated in four places along the profile (two basin columns at 360 km and 960 km and two crustal columns at 580 km and 655 km). The basin

columns were found to have higher average density than the surrounding crust indicating that the Moho upwarp may be overcompensating the mass of the basin at 360 km and 960 km. Another indication that this is the case is the presence of a small gravity high in a regional gravity low (810 km to 1090 km, Figure 3.15). The regional gravity low is likely a result of the low-density sediments in the Rome trough while the approximately 18 mGal relative high in the middle of it is due to the uplifted Moho bringing high-density mantle material closer to the surface.

Density variations within ND_NE are more drastic than ND_REFERENCE and ND_SW likely because this profile illustrates behavior not seen in the other two. The depth to the base of magnetization crosses the receiver functions/gravity based Moho at approximately 1000 km. As it is the deepest basin seen in all three profiles (approximately 7 km deep), this is not an unexpected response of the Moho to the lessened density of the overlying material. This boundary crossing is an interesting feature, and whether or not it is due to the margin of error of both datasets or is an actual geologically-derived feature is difficult to determine. Both the depth to the Moho from the receiver functions constrained by gravity and the depth to the base of magnetization have an error bar of ±5 km at this depth and since the difference in them is > 12 km at 1200 km location, the crossover could be real and the uppermost mantle in the region could be magnetic.

D. Inferences from Gravity Modeling

Inferences on the types of rocks at various levels within the crust can be drawn from the densities created by inversion. While the values for all three profiles are different from one another due to their unique crustal geometries, certain patterns do appear. Average densities of the upper (including intrusions), middle, and lower crustal blocks were calculated for all three models. Upper crustal average densities of 2743 kg/m^3 for ND_SW, 2737 kg/m^3 for ND_NE, and 2714 kg/m^3 for ND_REFERENCE were calculated. Average middle crustal densities are 2821 kg/m^3 for ND_SW, 2815 kg/m^3 for ND_REFERENCE, and 2807 kg/m^3 for ND_NE. Finally lower crustal average densities are 2967 kg/m^3 for ND_SW, 2950 kg/m^3 for ND_REFERENCE, and 2919 kg/m^3 for ND_NE (Table 4.2). With increasing depth there is increasing density. Extending from 26 km and down to the Moho, densities become more varying. Some profile require their

deepest crustal blocks (Figure 3.15, 260 km, 37 km depth) to have densities less than or equal 2900 kg/m^3 in order to compensate for the elevated high density (3300 kg/m^3) Moho whereas at other positions on the same profile (Figure 3.15, 780 km, 55 km depth), a depressed Moho yields higher densities within the lower crust (up to 3100 kg/m^3). This could indicate the presence of highly mafic and metamorphosed rocks such as gabbro or mafic amphibolitic to granulitic facies crustal rocks that have experienced an increase in density with continual burial deeper into the crust (Figure 3.10) (Gebrande, 1982; Ravat et al., 1999; Hinze et al., 2013).

Table 4.1 Average Middle Crustal Susceptibilities

Profile	Paleopro. (TDM>1.7 Ga)	Paleopro. (1.7Ga>TDM >1.55Ga)	Mesopro. (1.55Ga>TD M>1.3Ga)	Grenville (TDM<1.3Ga)
ND_SW	0.03 SI	0.06 SI	0.01 SI	0.009 SI
ND_REFERENCE	0.07 SI	0.04 SI	0.01 SI	0.02 SI
ND_NE	0.06 SI	0.07 SI	0.02 SI	0.009 SI
Average susceptibility for each time period	0.05 SI	0.06 SI	0.01 SI	0.01 SI

	T_{DM}>1.55Ga	T_{DM}<1.55Ga
Overall average susceptibility (SI)	0.06	0.01 SI

Table 4.2 Average Crustal Densities

Profile	Upper Crust Average Density (kg/m3)	Middle Crust Average Density (kg/m3)	Lower Crust Average Density (kg/m3)
ND_SW	2743	2821	2967
ND_REFERENCE	2714	2815	2950
ND_NE	2737	2807	2919

Chapter 5 Conclusion and Suggestions for Future Works

Laurentia has had a long and complex geological past. Modeling of the Paleoproterozoic zone of high magnetization is the first step toward understanding its origin. Low-pass filtered magnetic data show a long-wavelength magnetic anomaly high over the Paleoproterozoic side of the Nd T_{DM} line defined by Van Schmus et al. (1996) through the midcontinent of the United States. The magnetic high also coincides approximately with the boundaries of the Mazatzal province demarcated by Whitmeyer and Karlstrom (2007). In this study, the zone of high magnetization was modeled with gravity and magnetic anomalies using available constraints from geology and geophysics (rock types in the crystalline basement, the sedimentary thickness, the crustal thickness from USArray receiver functions constrained by gravity, and the base of magnetization) from across the T_{DM} line with three separate potential source scenarios (crust-only, mafic mantle underplating, and preserved magnetite from past mantle serpentinization).

Of the three scenarios, crust-only magnetization appears to be the most plausible even though the once-serpentinized mantle source may also be potentially valid. However, the crust-only model is slightly preferable due to its simplicity and lack of reliance on mantle sources for formation of the zone of high magnetization as continental mantle is generally considered non-magnetic (Wasilewski et al., 1979; Wasilewski and Mayhew, 1992). ND_REFERENCE calculated magnetic anomaly profile matches the observed without a mantle source. ND_SW and ND_NE calculated magnetic anomaly profiles in the zone of high magnetization did not fully match the observed. Because upper crustal intrusions were only modeled to the top of crystalline basement, it is likely that this is the cause of the mismatch between observed and calculated. If these intrusions were allowed to penetrate sedimentary rocks, the calculated magnetic anomaly would match the observed. Upper crustal intrusions are observed in the midcontinent region, in particular, the Green Island Plutonic Belt in southwestern Iowa that is of Mesoproterozoic crystallization age. Sm-Nd analysis of samples from these rocks indicates intrusion through older continental crustal of Paleoproterozoic (Mazatzal) age (Holm, 2007; Van Schmus et al., 1993, Van Schmus et al., 1996). Additionally, a series of near surface dike complexes were observed in Illinois and Indiana including intrusives in Hicks Dome and Omaha Dome (Hildenbrand and Ravat, 1997).

All three profiles display a similar trend in regards to magnetization. The lower crust is non-magnetic (from the base of magnetization estimates) in much of the Mesoproterozoic and older provinces in the region investigated. In the middle crust, higher susceptibilities exist in the older Paleoproterozoic and late Archean parts of the profiles (T_{DM}>1.55Ga). These range from 0.03 SI to 0.07 SI with an overall average for all three profiles at 0.06 SI. The Mesoproterozoic and Grenville terranes (T_{DM}<1.55Ga) range from 0.009 to 0.02 SI with an overall average of 0.01 SI (Table 4.1). Suture zones based on the maps of Whitmeyer and Karlstrom (2007) and Bickford et al. (2015) located along the Nd T_{DM} line separating the Paleoproterozoic (T_{DM}>1.55Ga) and Mesoproterozoic (T_{DM}<1.55Ga) are better modeled as one to two middle crustal blocks of low susceptibility (0.001 SI). The zones of severe deformation of rocks near the sutures may have been partly responsible for lowering the susceptibilities. The lowest modeled susceptibilities (0.009 SI) are found in the Grenville terranes.

All datasets used in the creation of the models inherently contain a margin of error. For the depth to the Moho this is approximately +/- 5-10 km (Chulick and Mooney, 2002). The depth to the base of magnetization is +/- 5km (D. Ravat, 2017, pers. comm.). The sedimentary thickness map also has a relatively similar margin of error away from drillholes (H. L. Zhang, 2017, pers. comm.).

The geodynamical origin responsible for the formation of the zone of high magnetization for these profiles is different from previously scenarios for late Paleoproterozoic Laurentia (Van Schmus et al., 1996) as they require westward dipping subduction instead of eastward (Figure 1.4). Previous geochemical models suggested eastward dipping subduction in order to provide a mechanism for creation of the island arc material geochemically found from rock samples in the midcontinent (Van Schmus, 2016, pers. comm.). However, westward dipping subduction in front of Grenville terranes could also explain Mesoproterozoic arcs. Westward dipping subduction under the southeastern Laurentian craton provides a mechanism for both serpentinization of the forearc mantle and mafic underplating. Without metasomatization brought on by dehydration of the subducting slab, neither of the two mantle scenarios could occur under the Paleoproterozoic margin. The stark magnetic susceptibility difference between Paleoproterozoic (T_{DM}>1.55Ga) and Mesoproterozoic (T_{DM}<1.55Ga) terranes is defined

by the T_{DM} age boundary. This sharp truncation of the zone of high magnetization at this boundary indicates the feature is unique to the Paleoproterozoic (T_{DM}) margin of Laurentia and unrelated to the later Mesoproterozoic (T_{DM}) arcs. Additionally, if mantle sources are not required to produce the high susceptibility, westward accretion of high susceptibility island arcs or intervening terranes on to the Laurentian margin provides an explanation for how they got there and why the terrane ends so abruptly on the southeastern side. This continuous accretion of arc material eventually formed the Mazatzal province (Amato et al., 2008; Whitmeyer and Karlstrom, 2007). The northwestern side of the high magnetization zone, which in this region corresponds to the Mazatzal terrane, is less well-defined than the southeastern edge. This suggests a hiatus in the terrane amalgamation, which is consistent with geochemical evidence of Nd T_{DM} boundary.

The geodynamical setting previously described to account for the creation of zone of high magnetization could also account for the Eastern Granite-Rhyolite province. Figure 1.4 illustrates rapid slab roll-back and break off from 1.4Ga to 1.36Ga. The roll-back of a westward-subducting slab would provide a mechanism for rapid transfer of heating of the lower crust in the Paleoproterozoic to the Mesoproterozoic side. The Eastern and Southern Granite-Rhyolite provinces were created diachronously, with the Eastern approximately 100 million years older than the Southern (1.45 Ga and 1.35 Ga, respectively). The succession of subducting slabs under Laurentian could have begun roll-back at the northern end and then proceeded south.

Additional basement core samples in currently unsampled areas with geochemical analysis of their TDM ages would provide greater information about the midcontinent. The lack of sample coverage for the area modeled provided one of the largest hurdles as there is little direct information concerning the nature of the rocks in the region. Additional Sm-Nd geochemical analysis of new samples from central Illinois would be useful as data from this region is lacking in the literature. In the meantime, magnetization boundaries and widening and narrowing of magnetization zones can help define physical terrane boundaries and understand the Proterozoic accretionary history of Laurentia. The susceptibility variation derived from the low-pass filtered or upward continued anomalies could help extend this interpretation to the south of this region into

OK-TX and in the Southern Granite-Rhyolite provinces where Rohs and Van Schmus (2007) have extended the mapped extent of the Nd TDM line. Finally, higher resolution tomographic models could better define the structure of the entire crust and help to distinguish the boundary between the northwestern Paleoproterozoic and southeastern Mesoproterozoic terranes.

Appendix: List of Values Used to Create ND_REFERENCE. Some of the block densities are inverted and hence have a decimal in significant digits.

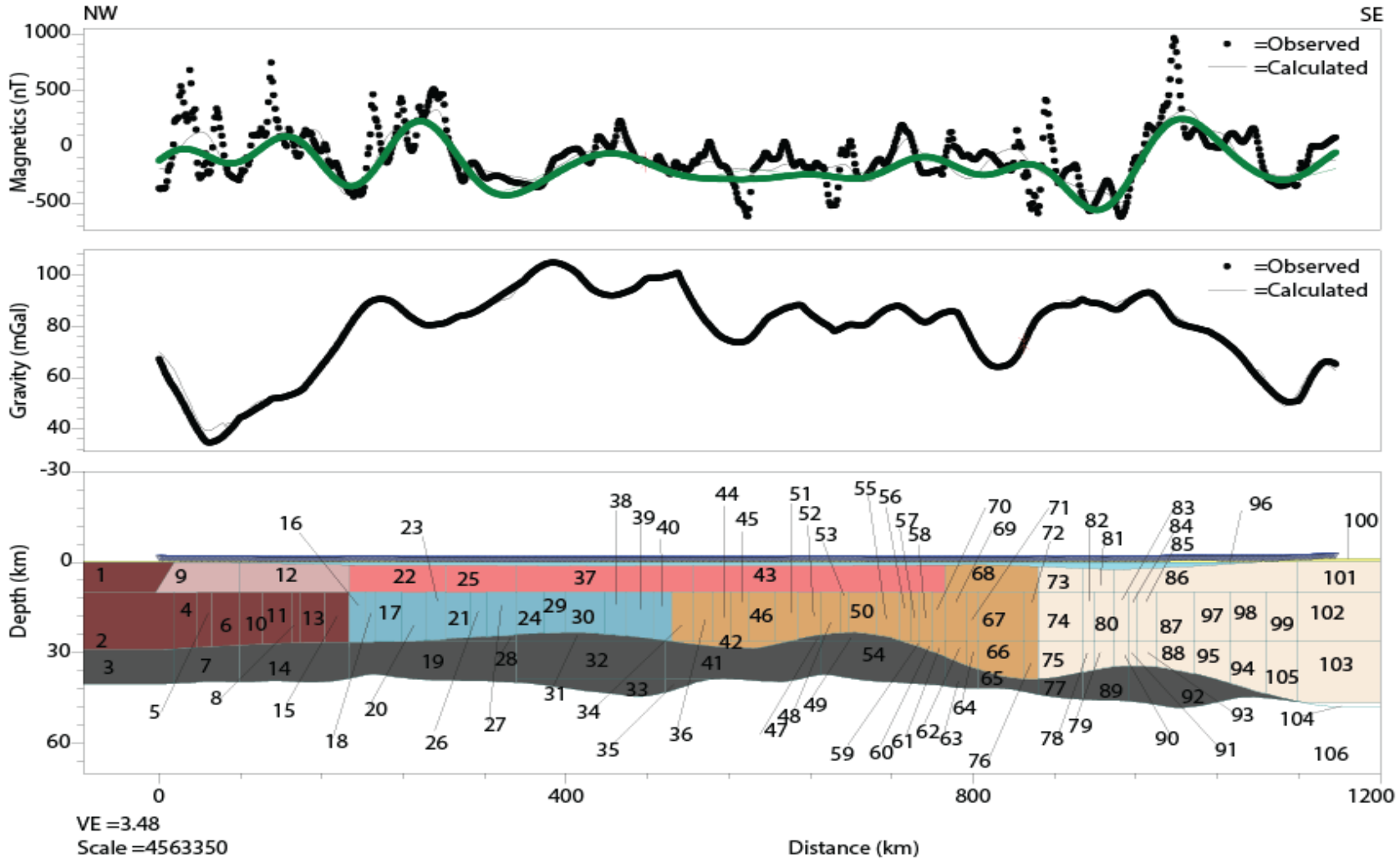

Block Label ND_REFERENCE_BWL100km	Density (kg/m^3)	Susceptibility (SI)
1	2700	0.01
2	2808.7	0.06
3	2950	0
4	2752.9	0.09
5	2660.7	0.09
6	2741	0.06
7	2900	0
8	2750	0.07
9	2720.1	0.01
10	2786.6	0.08
11	2775.9	0.09
12	2702.2	0.01
13	2783.1	0.08
14	2900	0
15	2788.5	0.02
16	2850.8	0.04
17	2836.7	0.09
18	2797.2	0.06
19	2900	0
20	2791.7	0.08
21	2819	0.001
22	2700	0.01
23	2800	0.08
24	2787.9	0.01
25	2700	0.01
26	2809.9	0.02
27	2838.4	0.01
28	2850	0
29	2838.8	0.03
30	2810.6	0.04
31	2900	0
32	2950	0
33	3000	0
34	2849.7	0.001
35	3000	0
36	2819.3	0.01
37	2750	0.01
38	2803.6	0.04
39	2839.4	0.01

40	2856.1	0.001
41	2900	0
42	2900	0.01
43	2700	0.01
44	2806	0.001
45	2782.5	0.001
46	2800	0.001
47	2807.5	0
48	2785.6	0.01
49	2800	0
50	2800	0.001
51	2847.8	0.01
52	2810.2	0.005
53	2796.9	0.02
54	2900	0
55	2850	0.03
56	2850	0.05
57	2850	0.02
58	2800	0.01
59	2900	0.02
60	2900	0.001
61	2900	0
62	2950	0.001
63	3000	0
64	2950	0.002
65	3100	0
66	2850	0.02
67	2796.2	0.02
68	2700	0.01
69	2850	0.001
70	2850	0.02
71	2800	0.001
72	2850	0.001
73	2700	0.01
74	2857.9	0.001
75	2950	0.001
76	2950	0.001
77	3100	0
78	2950	0.001
79	2950	0.01
80	2853.2	0.01

81	2700	0.001
82	2865.9	0.01
83	2800	0.001
84	2850	0.04
85	2850	0.07
86	2750	0.01
87	2846.3	0.07
88	2900	0.07
89	3100	0
90	2950	0.03
91	2950	0.07
92	3100	0
93	2950	0.07
94	2950	0.01
95	2950	0.04
96	2600	0
97	2842.8	0.04
98	2845	0.01
99	2791.7	0.01
100	-70	0
101	2750	0.01
102	2837	0.02
103	2957.5	0.02
104	3300	0
105	2818.9	0.01
106	3300	0

References

Allen, D.J., 1990, The Wisconsin gravity minimum: Source and implications [M.S. thesis]: West Lafayette, Indiana, Purdue University.

Allen, D.J., and W.J. Hinze (1992), Wisconsin gravity minimum: Solution of a geologic and geophysical puzzle and implications for cratonic evolution, *Geology*, **20**, 515-518, doi: 10.1130/0091-7613(1992)020<0515:WGMSOA>2.3.CO;.

Amato, J.M, A.O. Boullion, A.M. Serna, A.E. Sanders, G.L. Farmer, G.E. Gehrels, and J.L. Wooden (2008), Evolution of the Mazatzal province and the timing of the Mazatzal orogeny: Insights from U-Pb geochronology and geochemistry of igneous and metasedimentary rocks in southern New Mexico, *GSA Bulletin*, **120**(3/4), 328-346, doi: 10.1130/B26200.1.

Bankey, V., A. Cuevas, D. Daniels, C.A. Finn, I. Hernandez, P. Hill, R. Kucks, W. Miles, M. Pilkington, C. Roberts, W. Roest, V. Rystrom, S. Shearer, S. Snyder, R. Sweeney, J. Velez, J.D. Philips, and D. Ravat (2002), Digital data grids for the magnetic anomaly map of North America, *North American Magnetic Anomaly Group* (*NAMAG*).

Bickford, M.E., and B.M. Hill (2006), Does the arc accretion model adequately explain the Paleoproterozoic evolution of southern Laurentia?: An expanded interpretation, *Geology*, **35**(2), 167-170, doi: 10.1130/G23174A.1.

Bickford, M.E., W.R. Van Schmus, and I. Zietz (1986), Proterozoic history of the midcontinent region of North America, *Geology*, **14**(6)**,** 492-496, doi: 10.1130/0091-7613(1986)14<492:PHOTMR>2.0.CO;2.

Bickford, M.E., W.R. Van Schmus, K.E. Karlstrom, P.A. Mueller, and G.D. Kamenov (2015), Mesoproterozoic-trans-Laurentian magmatism: A synthesis of continent-wide age distributions, new SIMS U–Pb ages, zircon saturation temperatures, and Hf and Nd isotopic compositions, *Precambrian Research*, **265**(2015), 286-312, doi: 10.1016/j.precamres.2014.11.024.

Blakely, R.J (1996), Potential theory in gravity and magnetic applications, *Cambridge University Press*.

Blakely, R.J., T.M Brocher, and R.E. Wells (2005), Subduction-zone magnetic anomalies and implications for hydrated forearc mantle, *Geology*, **33**(6), 445-448, doi: 10.1130/G21447.1.

Bostock, M.G., R.D. Hyndman, S. Rondenay, and S.M. Peacock (2002), An inverted continental Moho and serpentinization of the forearc mantle, *Letters to Nature*, **417**, doi: 10.1038/417536a.

Carr, S.D., R.M. Easton, R.A. Jamieson, and N.G. Culshaw (2000), Geologic transect across the Grenville orogeny of Ontario and New York, *Canadian Journal of Earth Science*, **37**(2000), 193-216, doi: 10.1139/e99-074.

Cawood, P.A., A. Kröner, W.J. Collins, T.M. Kusky, W.D. Mooney, and B.F. Windley (2009), Accretionary orogens through Earth history in: Cawood P.A., Kröner A. (Eds.), *Earth Accretionary Systems in Space and Time, Geological Society of London Special Publication*, **318**, 1–36, doi: 10.1144/SP318.1.

Chandler, V.W., and K.C. Malek (1991), Moving-window Poisson analysis of gravity and magnetic data from the Penokean orogeny, east-central Minnesota, *Geophysics*, **56**(1), 123-132, doi: 10.1190/1.1442948.

Chulick, G.S., and W.D. Mooney (2002), Seismic structure of the crust and uppermost mantle of North America and adjacent oceanic basins: a synthesis, *Bulletin of the Seismological Society of America*, **92**(6), 2478-2492.

Clark, D.A. (1997), Magnetic petrophysics and magnetic petrology: aids to geological interpretation of magnetic surveys, *AGSO Journal of Australian Geology and Geophysics*, **17**(2), 83-103.

Clark, D.A. (1999), Magnetic petrology of igneous intrusions: implications for exploration and magnetic interpretation, *Exploration Geophysics*, **30**, 5-26, doi: 10.1071/EG999005.

Clark, D.A. (2014), Methods for determining remanent and total magnetisations of magnetic sources – a review, *Exploration Geophysics*, **45**, 271-304, doi: 10.1071/EG14013.

Clark, D.A., and D.W. Emerson (1991), Notes on rock magnetization characteristics in applied geophysics studies, *Exploration Geophysics*, **22**(1991), 547-565, doi: 10.1071/EG991547.

Craddock, J.P., and A.W. McKiernan (2007), Tectonic implications of finite strain variations in Baraboo-interval quartzites (ca. 1700 Ma), Mazatzal orogeny, Wisconsin and Minnesota, USA, *Precambrian Research*, **156**(2007), 175-194, doi: 10.1016/j.precamres.2006.03.010.

Davidson, A. (2008), Late Paleoproterozoic to mid-Neoproterozoic history of northern Laurentia: An overview of central Rodinia, *Precambrian Research*, **160**(2008), 5-22, doi: 10.1016/j.precamres.2007.04.023.

DePaolo, D.J., and G.J. Wasserburg (1976), Nd isotopic variations and petrogenentic models, *Geophysical Research Letters*, **3**(5), 249-252, doi: 10.1029/GL003i005p00249.

Duebendorfer, E.M., M.L. Williams, and K.R. Chamberlain (2015), Case for a temporally and spatially expanded Mazatzal orogeny, *Lithosphere*, **7**(6), 603-610, doi: 10.1130/L412.1.

Ellett, K.M., and Naylor, S., 2016, Utility of geological and pedological models in the design of geothermal heat pump systems, *in* Dowling, C.B., Neumann, K., and Florea, L.J., eds., Geothermal Energy: An Important Resource, *Geological Society of America Special Paper 519*, 1–17, doi:10.1130/2016.2519(01).

Fisher, C.M., S.L Loewy, C.F. Miller, P. Berquist, W.R. Van Schmus, R.D. Hatcher, J.L. Wooden, and P.D. Fullagar (2010), Whole-rock Pb and Sm-Nd isotopic constraints on the growth of southeastern Laurentia during Grenvillian orogenesis, *GSA Bulletin*, **122**(9-10), 1646-1659, doi: 10.1130/B30116.1.

Fyfe, W.S. (1991), Magma underplating of continental crust, *Journal of Volcanology and Geothermal Research*, **50**(1992), 33-40, doi: 10.1016/0377-0273(92)90035-C.

Gebrande, H. (1982), Elastic wave velocities and constants of elasticity of rocks at room temperature and pressures < 1 GPa, *in* 3.1 Elastic wave velocities and constants of elasticity of rocks and rock forming minerals, ed. G. Angenheister.

Goodge, J.W., and J.D. Vervoort (2006), Origin of Mesoproterozoic A-type granites in Laurentia: Hf isotope evidence, *Earth and Planetary Science Letters*, **243**(2006), 711-731, doi: 10.1016/j.epsl.2006.01.040.

Green, T.H., and A.E. Ringwood (1968), Genesis of the calc-alkaline igneous rock suite, *Contributions to Mineralogy and Petrology*, **18**(2), 105-12, doi: 10.1007/BF0037180.

Hawkins, J.W., S.H. Bloomer, C.A. Evans, and J.T. Melchior (1984), Evolution of intra-oceanic arc-trench systems, *Tectonophysics*, **102**(1984), 175-205, doi: 10.1016/0040-1951(84)90013-1.

Hildenbrand, T.G., and D. Ravat (1997), Geophysical setting of the Wabash Valley Fault System, *Seismological Research Letters*, **68**(4), 567-585, doi: 10.1785/gssrl.68.4.567.

Hinze, W.J., R.R.B. von Frese, and A.H. Saad (2013), Gravity and magnetic exploration: principles, practices, and applications, Cambridge University Press, Cambridge, in press.

Hunt, C.P., B.M. Moskowitz, and S.K. Banerjee (1995), Magnetic properties of rocks and minerals, *in* Rock Physics & Phase Relations: A Handbook of Physical Constants (ed T. J. Ahrens), *American Geophysical Union*, Washington, D.C., doi: 10.1029/RF003p0189.

Hyndman, R.D., and S.M. Peacock (2003), Serpentinization of the forearc mantle, *Earth and Planetary Science Letters*, **212**, 417-432, doi: 10.1016/S0012-821X(03)00263-2.

Karlstrom, K.E., J.M. Amato, M.L. Williams, M. Heizler, C.A. Shaw, A.S. Read, and P. Bauer (2004), Proterozoic tectonic evolution of the New Mexico region, *in* Mack, G.H., and Giles, K.A., eds., *The Geology of New Mexico: A Geologic history*: *New Mexico Geological Society Special Publication*, **11**, 1–34.

Kirby, S.H., S. Stein, E.A. Okal, and D.C. Rubie (1996), Metastable mantle phase transformations and deep earthquakes in subducting oceanic lithosphere, *Reviews of Geophysics*, **34**(2), 261-306, doi: 10.1029/96RG01050.

Kodaira, S., S. Takeshi, N. Takahashi, S. Miura, Y. Tamura, Y. Tatsumi, and Y. Kaneda (2007), New seismological constraints on growth of continental crust in the Izu-Bonin intra-oceanic arc, *Geology*, **35**(11), 1031-1034, doi: 10.1130/G23901A.1.

Laske, G, G. Masters, Z. Ma, M.E., Pasyanos (2012), CRUST1.0: An updated global model of Earth's crust, EGU2012-3743-1, *Geophys Res Abs*.

Liu, Q., B.R. Frost, H. Wang, J. Zheng, Q. Zeng, and Z. Jin (2012), Magnetic petrology of high Fe-Ti eclogites from the CCSD main hole: Implications for subduction-zone magnetism, *Journal of Geophysical Research*, **117**, doi: 10.1029/2011JB008621.

Lowry, A.R., and M. Perez-Gussinye (2011), The role of crustal quartz in controlling Cordilleran deformation, *Nature*, **471**, 353-357, doi: 10.1038/nature09912.

Lucius, J.E., and R.R.B. Von Frese (1988), Aeromagnetic and gravity anomaly constrains on the crustal geology of Ohio, *GSA Bulletin*, **100**(1), 104-116, doi: 10.1130/0016-7606(1988)100<0104:AAGACO>2.3.CO;2.

Marshall, E.W., J.C. Lassiter, J.D. Barnes, A. Luguet, and M. Lissner (2017), Mantle melt production during the 1.4 Ga Laurentian magmatic event: Isotopic constraints from Colorado Plateau mantle xenoliths, *Geology*, doi:10.1130/G38891.1.

Meert, J.G. (2002), Paleomagnetic evidence for a Paleo-Mesoproterozoic supercontinent Columbia, *Gondwana Resesarch*, **5**(1), 207-215, doi:10.1016/S1342-937X(05)70904-7.

Mooney, W.D., and M.K. Kaban (2010), The North American upper mantle: Density, composition, and evolution, *Jounral of Geophysical Research*, **115**(B12), 2156-2202, doi: 10.1029/2010JB000866

Mosher, S., J.S.F. Levine, and W.D. Carlson (2008), Mesoproterozoic plate tectonics: A collisional model for the Grenville-aged orogenic belt in the Llano uplift, central Texas, *Geology*, **36**, 55-58, doi: 10.1130/G24049A.1.

Negredo, A.M., J.L Valera, and E. Carminati (2004), TEMSPOL: a MATLAB thermal model for deep subduction zones including major phase transformations, *Computers & Geosciences*, **30**, 249-258, doi:10.1016/j.cageo.2004.01.002.

Nelson, B.K., and D.J. DePaolo (1985), Rapid production of continental crust 1.7 to 1.9 b.y. ago: Nd isotope evidence from the basement of the North American mid-continent, *GSA Bulletin*, **96**, 746-754, doi: 10.1130/0016-7606(1985)96<746:RPOCCT>2.0.CO;2.

Pilkington, M., and J.A. Percival (1999), Crustal magnetization and long-wavelength aeromagnetic anomalies of the Minto block, Quebec, *Journal of Geophysical Research*, **104**(B4), 7513-7526, doi: 10.1029/1998JB900121.

Ranero, C.R., J.P. Morgan, K. McIntosh, and C. Reichert (2003), Bending-related faulting and mantle serpentinization at the Middle America trench, *Nature*, **425**, 367-373, doi: 10.1038/nature01961.

Ravat, D. (2007), Crustal magnetic fields, *Encyclopedia of Geomagnetism and Paleomagnetism, D. Gubbins and E. Herrero-Bevera (eds.)*, 140-144.

Ravat, D., Finn, C., Hill, P., Kucks, R., Phillips, J., Blakely, R., Bouligand, C., Sabaka, T., Elshayat, A., Aref, A., and Elawadi, E. (2009), A preliminary, full spectrum, magnetic anomaly grid of the United States with improved long wavelengths for studying continental dynamics--A website for distribution of data, *U.S. Geological Survey Open-File Report*, 2009–1258, 2 p.

Ravat, D., T.G. Hildenbrand, and W. Roest (2003), New way of processing near-surface magnetic data: The utility of the Comprehensive Model of the Magnetic Field, *The Leading Edge*, **22**(8), 784-785, doi: 10.1190/1.1605082.

Ravat, D., P. Morgan, and A.R. Lowry (2016), Geotherms from the temperature-depth–constrained solutions of 1-D steady-state heat-flow equation, *Geosphere*, **12**(4), doi: 10.1130/GES01235.1.

Ravat. D, Z. Lu, and L.W. Braile (1999), Velocity–density relationships and modeling the lithospheric density variations of the Kenya Rift, *Tectonophysics*, **302**(1999), 225-240, doi: 10.1016/S0040-1951(98)00283-2.

Ravat, D., A. Pignatelli, I. Nicolosi, and M. Chiappini (2007), A study of spectral methods of estimating the depth to the bottom of magnetic sources from near-surface magnetic anomaly data, *Geophysical Journal International*, **169**(2), 421-434, doi: 10.1111/j.1365-246X.2007.03305.x.

Ravat, D., H.L. Zhang, L.C. Newman, and A.R. Lowry (2015), New insights into the tectonics of the midcontintent of U.S.A. from EarthScope USArray seismic, gravity, magnetic and heat flow datasets, Abstract T11C-2907 presented at 2015 Fall Meeting, AGU, San Francisco, Calif., 14-18 Dec.

Rivers, T. (1997), Lithotectonic elements of the Grenville Province: review and tectonic implications, *Precambrian Research*, **86**(1997), 117-154, doi: 10.1016/S0301-9268(97)00038-7

Rogers, J.W., and M. Santosh (2002), Configuration of Columbia, a Mesoproterozoic supercontinent, *Gondwana Research*, **5**(1), 5-22, doi:10.1016/S1342-937X(05)70883-2.

Rohs, C.R., and W.R. Van Schmus (2007), Isotopic connections between basement rocks exposed in the St. Francois Mountains and the Arbuckle Mountains, southern mid-continent, North America, *Int J Earth Sci (Geol Rundsch)*, **95**, 599-611, doi: 10.1007/s00531-006-0123-5.

Rudnick, R.L., and D.M. Fountain (1995), Nature and composition of the continental crust: A lower crustal perspective, *Reviews of Geophysics*, **33**(3), 267-309, doi: 10.1029/95RG01302.

Sabaka, T.J., N. Olsen, M.E. Purucker (2004), Extending comprehensive models of the Earth's magnetic field with Ørsted and CHAMP data, *Geophys. J. Intl.*, **159**(2004), 521-547, doi: 10.1111/j.1365-246X.2004.02421.x

Salem, A., C. Green, D. Ravat, K.H. Singh, P. East, J.D. Fairhead, S. Mogren, and E. Biegert (2014), Depth to Curie temperature across the central Red Sea from magnetic data using the de-fractal method, *Tectonophysics*, **624–625**(2014), 75–86, doi: 10.1016/j.tecto.2014.04.027.

Schmandt, B., F. Lin, and K.E. Karlstrom (2015), Distinct crustal isostasy trends east and west of the Rocky Mountain Front, *Geophysical Research Letters*, **42**, 10,290-10298, doi: 10.1002/2015GL066593.

Singh, B. (2002), Simultaneous computation of gravity and magnetic anomalies resulting from a 2-D object, *Geophysics,* **67**(3), 801-806, doi: 10.1190/1.1484524.

Singh, B., and D. Guptasarama (2001), New method for fast computation of gravity and magnetic anomalies from arbitrary polyhedral, *Geophysics*, **66**(2), 521-526, doi: 10.1190/1.1444942.

Slagstad, T., N.G. Culshaw, J.S. Daly, and R.A. Jamieson (2009), Western Grenville Province holds key to midcontinental Granite-Rhyolite Province enigma, *Terra Nova*, **21**, 181-187, doi: 10.1111/j.1365-3121.2009.00871.x.

Stein, C.A., J. Kley, S. Stein, D. Hindle, and G.R. Keller, (2015), North America's midcontinent Rift: When rift met LIP, *Geosphere*, **11**(5), 1607–1616, doi:10.1130/GES01183.1.

Stern, R. J., Fouch, M. J. and Klemperer, and S. L. (2004), An overview of the Izu-Bonin-Mariana subduction factory, in *Inside the Subduction Factory (ed J. Eiler), American Geophysical Union*, doi: 10.1029/138GM10.

Talwani, M., and J.R. Heirtzler (1964), Computation of magnetic anomalies caused by two-dimensional bodies of arbitrary shape, *Computers in the mineral industries, Part 1: Stanford Univ. Publ., Geological Sciences*, **9**, 464-480, doi: 10.1111/j.1365-246X.1969.tb03568.x.

Thomas, M.D., V.L. Sharpton, and R.A.F. Grieve (1987), Gravity patterns and Precambrian structure in the North American Central Plains, *Geology*, **15**, 489-492, doi: 10.1130/0091-7613(1987)15<489:GPAPSI>2.0.CO;2.

Thybo, H., and I.M. Artemieva (2013), Moho and magmatic underplating in continental lithosphere, *Tectonophysics*, **609**(2013), 605-619, doi: 10.1016/j.tecto.2013.05.032.

Toft, P.B., J. Arkani-Hamed, and S.E. Haggerty (1990), The effects of serpentinization on density and magnetic susceptibility: a petrophysical model, *Physics of the Earth and Planetary Interiors*, **65**(1990), 137-157, doi: 10.1016/0031-9201(90)90082-9.

Van Schmus, W.R., Bickford, M.E., Condie, K., (1993), Early Proterozoic crustal evolution. In: Reed Jr., J.C., et al. (Eds.), *Precambrian: Conterminous U.S. Geol. Soc. North Am. C-2*, 270–281.

Van Schmus, W.R., M.E. Bickford, and A. Turek (1996), Proterozoic geology of the east-central midcontinent basement, *in* van der Pluijm, B.A., and Catacosinos, P.A., eds, Basement and Basins of Eastern North America: Boulder, Colorado, *Geol. Soc. Am. Special Paper*, **308**, 7–32.

Van Schmus, W.R., D.A. Schneider, D.K. Holm, S. Dodson, and B.K. Nelson (2007), New insights into the southern margin of the Archean-Proterozoic boundary in the north-central United States based on U-Pb, Sm-Nd, and Ar-Ar geochronology, *Precambrian Research*, **157**, 80-105, doi:10.1016/j.precamres.2007.02.011.

Wasilewski, P.J., and M.A. Mayhew (1992), The Moho as a magnetic boundary revisited, *Geophysical Research Letters*, **19**(22), 2259-2262, doi: 10.1029/92GL01997.

Wasilewski, P.J., H.H. Thomas, and M.A. Mayhew (1979), The Moho as a magnetic boundary, *Geophysical Research Letters*, **6**(7), 541-544, doi: 10.1029/GL006i007p00541.

Whitmeyer, S.J., and K. Karlstrom (2007), Tectonic model for the Proterozoic growth of North America, *Geosphere*, **3**(4), 220-259, doi: 10.1130/GES00055.1.

Yuan, H., S. French, P. Cupillard, and B. Romanowicz (2014), Lithospheric expression of geological units in central and eastern North America from full waveform tomography, *Earth and Planetary Science Letters*, **402**(2014), 176-186, doi: 10.1016/j.epsl.2013.11.057

Zandt, G., and J.A. Ammon (1995), Continental crust composition constrained by measurements of crustal Poisson's ratio, *Nature*, **374**(6099), 152-154, doi:

Zhao, G., M. Sun, S.A. Wilde, and S. Li (2004), A Paleo-Mesoproterozoic supercontinent: assembly, growth and breakup, *Earth-Science Reviews*, **67**, 91-123, doi:10.1016/j.earscirev.2004.02.003.

Zhao, G., P.A. Cawood, M. Sun, and S.A. Wilde (2002), Review of global 2.1–1.8 Ga orogens: implications for a pre-Rodinia supercontinent, *Earth-Science Reviews*, **59**, 125-162, doi: 10.1016/S0012-8252(02)00073-9.

Zhao, J., and M.T. McCulloch (1995), Geochemical and Nd isotopic systematics of granites from the Arunta Inlier, central Australia: implications for Proterozoic crustal evolution, *Precambrian Research*, **71**(1995), 265-299, doi: 10.1016/0301-9268(94)00065-Y.

Vita

Rachel Lauren Durham
Orlando, Florida

Education
University of Florida, B.S. Geology, 2015

Professional Positions
Teaching and Research Assistant, University of Kentucky, 2015-2017

Professional Publications
Durham, R.L., and D. Ravat (2016), On the Origin of the High Magnetization Zone Parallel to the Paleoproterozoic – Mesoproterozoic Southeastern Margin (Neodymium Line) of Laurentian United States, Abstract T31F-2990 presented at 2016 Fall Meeting, AGU, San Francisco, Calif., 12-16 Dec.

Scholastic and Professional Honors
Member of Sigma Gamma Epsilon Honor Society
Teaching Assistant of the Year Award, 2016